Role of the -PEWY-glutamate in catalysis at the Q_o-site of the Cyt bc_1 complex

Doreen Victoria [a,c], Rodney Burton [a], Antony R. Crofts [a,b,*]

[a] Department of Biochemistry, University of Illinois at Urbana-Champaign, Urbana, IL 61801, USA
[b] Center for Biophysics and Computational Biology, University of Illinois at Urbana-Champaign, Urbana, IL 61801, USA
[c] Roche Molecular Systems, Inc., 4300 Hacienda Dr., Pleasanton, CA 94588, USA

ARTICLE INFO

ABSTRACT

We re-examine the pH dependence of partial processes of ubihydroquinone (QH_2) turnover in Glu-295 mutants in *Rhodobacter sphaeroides* to clarify the mechanistic role. In more crippled mutants, the bell-shaped pH profile of wildtype was replaced by dependence on a single pK at ~8.5 favoring electron transfer. Loss of the pK at 6.5 reflects a change in the rate-limiting step from the first to the second electron transfer. Over the range of pH 6–8, no major pH dependence of formation of the initial reaction complex was seen, and the rates of bypass reactions were similar to the wildtype. Occupancy of the Q_o-site by semiquinone (SQ) was similar in the wildtype and the Glu→Trp mutant. Since heme b_L is initially oxidized in the latter, the bifurcated reaction can still occur, allowing estimation of an empirical rate constant $<10^3$ s^{-1} for reduction of heme b_L by SQ from the domain distal from heme b_L, a value 1000-fold smaller than that expected from distance. If the pK ~8.5 in mutant strains is due to deprotonation of the neutral semiquinone, with $Q^{\bullet-}$ as electron donor to heme b_L, then in wildtype this low value would preclude mechanisms for normal flux in which semiquinone is constrained to this domain. A kinetic model in which Glu-295 catalyzes H+ transfer from QH•, and delivery of the H+ to exit channel(s) by rotational displacement, and facilitates rapid electron transfer from SQ to heme b_L by allowing $Q^{\bullet-}$ to move closer to the heme, accounts well for the observations.

© 2012 Elsevier B.V. All rights reserved.

1. Introduction

The cytochrome (cyt) bc_1 complex (ubihydroquinone:cyt c oxidoreductse, E.C. 1.10.2.2, or complex III of the mitochondrial respiratory chain), catalyzes oxidation of ubihydroquinone (quinol, QH_2) by cyt c (or cyt c_2 in bacteria). The complex in both mitochondria and bacteria is a homodimer, with a catalytic core of three subunits, cyt b, cyt c_1, and the Rieske iron–sulfur protein (ISP), in each monomer. In bacterial complexes, no other subunits are structurally defined, but in *Rhodobacter sphaeroides*, the isolated complex has an additional subunit (SU IV) of uncertain function, which is absent from that of the closely related *Rb. capsulatus*. Mitochondrial complexes have up to 11 subunits, many of uncertain function [1,2].

In the Q-cycle mechanism through which the complex operates (Fig. 1), oxidation of QH_2 at the Q_o-site occurs through a bifurcated reaction delivering the electrons to two different acceptor chains [3–6]. The first electron reduces the high potential chain (ISP and cyt c_1), and generates an intermediate semiquinone (SQ). The electron from SQ reduces the low potential chain, consisting of hemes b_L and b_H of cyt b, which deliver the electron across the membrane to reduce ubiquinone (Q) or SQ at the Q_i-site in an electrogenic process that contributes to the electrical component of the proton gradient used to drive ATP synthesis.

In the first electron transfer, both an electron and a proton are transferred on reduction of ISP_{ox}, leaving as a product the neutral semiquinone, QH•. The proton-coupled electron transfer of this step accounts for the high activation energy of the overall reaction [7], and mechanistic parameters have been established from detailed studies of the dependence of rate on physicochemical properties of ISP [8–13]. The mechanism of the second electron transfer is more controversial. The Q-cycle operates with high efficiency so that in the absence of backpressure from the proton gradient [14], virtually all electrons go through the bifurcated process. If electron exit from the low potential chain is blocked, bypass reactions occur, which under aerobic conditions lead to reduction of O_2 to superoxide, and a cascade of secondary reactive oxygen species (ROS) and related radicals that lead to cellular damage, aging, etc. [15–17]. A question of mechanistic and anthropocentric interest is how evolution has honed the mechanism to minimize these damaging short-circuits.

1.1. Structural considerations

Structures at atomic resolution are available from mitochondrial and bacterial sources [18–23], but some aspects of the structure–
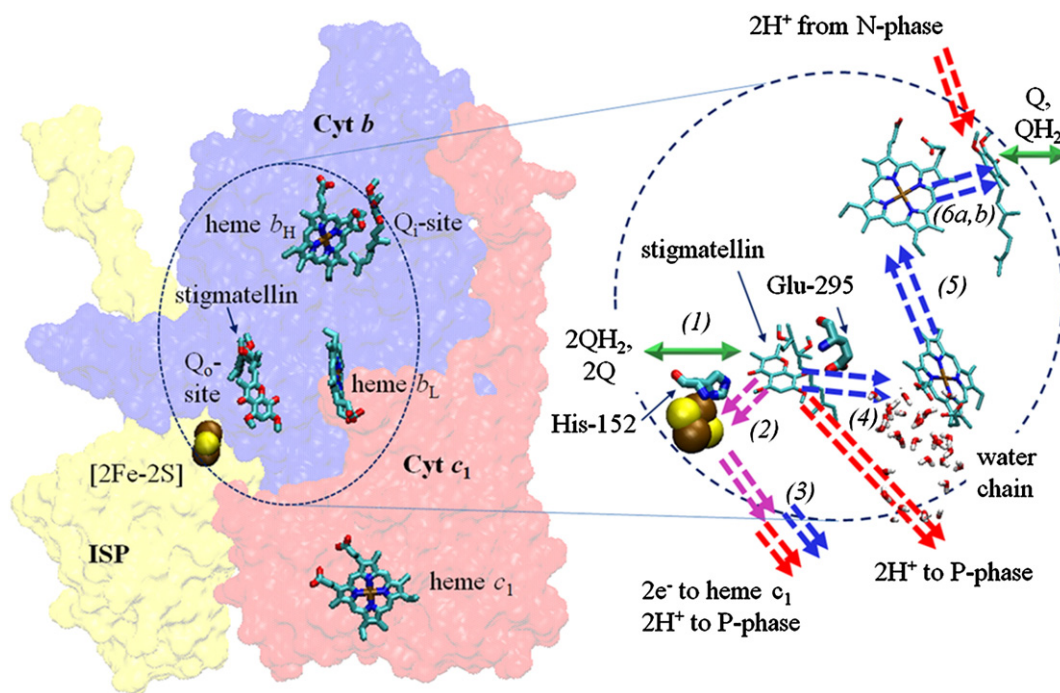
Fig. 1. Q-cycle mechanism. Left, the subunits of the *Rb. sphaeroides* bc_1 complex, and the prosthetic groups of importance in mechanism (taken from PDB ID: 2QJY). Right, the catalytic core rotated so as to display the main players. The reactions of the Q-cylce are shown by magenta arrows (H transfers), green arrows (Q, QH_2 exchange at catalytic sites), blue arrows (electron transfers) and red arrows (H^+ transfers). Stigmatellin bound at the Q_o-site shows the position at which the ES_1-complex forms. Reactions numbered are as follows:

Formation of ES_1-complex

$$Eb_Hb_L + QH_2 + ISP_{ox} \rightleftharpoons Eb_Hb_L \cdot QH_2 \cdot ISP_{ox} \tag{1}$$

High potential chain (1st e^- transfer and formation of ES_2-complex)

$$Eb_Hb_L \cdot QH_2 \cdot ISP_{ox} \rightleftharpoons ISPH + Eb_Hb_L \cdot QH^{\cdot} \tag{2}$$

$$ISPH + ferriheme \; c_1 \rightleftharpoons ISP_{ox} + ferroheme \; c_1 + H_P^+ \tag{3}$$

Low potential chain (2nd e^- transfer)

$$Eb_Hb_L \cdot QH^{\cdot} \rightleftharpoons Eb_Hb_L^- + Q + H_P^+ \tag{4}$$

$$Eb_Hb_L^- \rightleftharpoons Eb_H^- b_L \tag{5}$$

$$Eb_H^- b_L + Q + H_N^+ \rightleftharpoons Eb_Hb_LQ^{\cdot-}\left(H^+\right) \; or \; Eb_H^- b_LQ^{\cdot-}\left(H^+\right) + H_N^+ \rightleftharpoons Eb_Hb_L + QH_2 \tag{6a, 6b}$$

function interface can only be addressed through models because the enzyme-substrate (*ES*-) complexes for both Q_o-site electron transfers are metastable. Speculation about the mechanism of the initial step depends on the nature of its ES-complex (ES_1) at the Q_o-site (Fig. 1, Eq. (1)). The two substrates, QH_2 and ISP_{ox}, cannot coexist in equilibrium at any E_h; the driving force ($\Delta E'$) is generated in vivo by metabolism, or by activation of linked photochemical processes, and ES_1 has so far been inaccessible to crystallographic exploration. Models for the reaction complex have been based on the binding of inhibitors, well-defined in structures. In particular, that for stigmatellin has been used as a guide in discussion of both ES_1 and enzyme-product (*EP*-) complexes [24–26]. The protein side-chains liganding the inhibitor (His-152 of ISP and Glu-295 of cyt *b*, using *Rb. sphaeroides* numbering), have attracted particular attention. The ES_1-complex has been modeled by replacing stigmatellin with QH_2, which fits well within the electron density of the inhibitor [25]. However, the polarity of the H-bond between ISP and the occupant is different; His-152 of the reduced ISP (ISPH) is the H-bond donor to a carbonyl group of stigmatellin, while in ES_1 a phenolic -OH of QH_2 would donate an H-bond to ISP_{ox}, with

His-152 in the imidazolate form [8,13,27]. The difference in polarity largely reflects the change in p*K* of His-152 on reduction to give ISPH, which is fully protonated in the neutral range. NMR studies in *Thermus thermophilus* bc_1 complex [28] have now unambiguously associated the values for pK_{ox1} and pK_{ox2} with histidines equivalent to His-152 and His-131 of ISP, with values ~7.6 and ~9.6 in *Rb. sphaeroides*, while the pK_{red} values of both in ISPH are in the range ~12–13 [29].

1.2. The first electron transfer

At saturating substrate concentrations, the first electron transfer is a rate-limiting proton-coupled electron transfer, the reaction is endergonic [7,8,30–33], and the products are ISPH and the neutral semiquinone, $QH^{\bullet}$. The reaction is proton-first-then-electron; the rate depends on the contribution of pK_{ox1} of ISP to the Brønsted barrier determining distribution of the proton along the H-bond [34], and on the contribution of $E_{m,ISP}$ to the electron transfer driving force and activation barrier. The behavior is well-described according to a Marcus–Brønsted relationship [13,27,48], and varies on modification of these values in ISP

mutants. When substrates QH2 or ISPox were limiting, the rate also varied as expected from the controlling role for substrate concentration in formation of the ES_1-complex (Eqs. (1), (7), and (8)), such that with one substrate held constant at saturating concentration, variation of the other gave the Michaelis–Menten behavior [7] [35], allowing calculation of relative binding coefficients of both substrates:

$$Eb_Hb_L \cdot ISP_{ox} \xrightleftharpoons[K_{QH_2}]{QH_2} Eb_Hb_L \cdot QH_2 \cdot ISP_{ox}; K_{QH_2} = \exp\left\{\frac{zF}{RT}\Delta E_m^{ES-free}\right\} \quad (7)$$

$$Eb_Hb_L \cdot QH_2 \xrightleftharpoons[K_{ISP_{ox}}]{ISP_{ox}} Eb_Hb_L \cdot QH_2 \cdot ISP_{ox}; K_{ISP_{ox}} = 10^{(pK_{ox1}-pK_{app})} \quad (8)$$

The pH dependence of quinol oxidation shows an increase over the range pH 6 to 7, described by an apparent pK (pK_{app}) of ~6.5 [7]. We suggested that the difference between pK_{app} and pK_{ox1} ~7.6 (in wildtype) of the isolated ISP must reflect $K_{ISP_{ox}}$ (Eq. (8)), the binding constant for formation of the ES_1-complex. With ISP mutant strains, pK_{app} varied in parallel with change in pK_{ox1} [7,13], demonstrating a direct correlation.

1.3. The second electron transfer

The ES-complex (ES_2) for the second step (Eqs. (4)–(6a,6b)) is the bound QH• product of the first (Eq. (2)), and is also inaccessible to crystallography. In normal forward chemistry, the second electron transfer is fast enough to rapidly remove SQ so that none can be detected [36–38]. Different mechanisms have been proposed for this step, including variants of concerted mechanisms [31,39,40], double-gated mechanisms [41], double-occupancy mechanisms [42–44], SQ stabilized in a complex with ISPH [45,46], and low occupancy by SQ with rate enhanced by mobility [7,24,26]. This choice of mechanisms is representative of the controversy as to the state from which electron transfer to heme b_L occurs. We had suggested that an anionic species, $Q^{\bullet-}$, might migrate close to the heme so as to react rapidly at low occupancy [24,26,47,48]. As recently demonstrated by EPR [30,32,37], under conditions in which it can accumulate, SQ is retained in the Q_o-site volume as the anionic species $Q^{\bullet-}$ [30], likely with Glu-295 carboxylate as H^+ acceptor. The properties are in line with the mechanism proposed [24], but discrepancies between labs as to occupancy translate to uncertainties in interpretation of kinetic data.

The focus of the present study is Glu-295 of cyt b (E295), highly conserved in α-proteobacteria and mitochondria. The -PEWY- span containing this residue forms one side of the Q_o-site. Our previous studies had shown that mutagenesis resulted in strongly inhibited rates of QH2 oxidation, and as structures became available, an obvious explanation became apparent [24,49]. In stigmatellin-containing structures, the carboxylate group of E295 is H-bond acceptor from a hydroxyl group of the inhibitor [24,26]. In the native structure, and those occupied by myxothiazol (or several other similar MOA-type inhibitors with an E-β-methoxy-acrylamide (or -acrylate) active group), the side chain is rotated by some 160° [26,50] so that the carboxyl group connects to a water chain leading to the P-phase aqueous interface [21,24,26,51]. This difference in configuration suggested a functional role for E295 in removal of the second proton from quinol oxidation [21,24,51]. The E295 would accept a proton from the neutral QH• (formed in the first electron transfer) via the ring –OH, and deliver it by rotation of the (now) carboxylic sidechain to the proton exit channel, leaving the anionic $Q^{\bullet-}$ in the site. Clearly, mutation of E295 would be expected to lead to inhibition of this step. Dissociation and H^+ transfer down the water chain would then provide a pathway for exit to the P-phase. When stigmatellin occupied the site, structures show that the E295 side-chain and two water molecules filled the volume between the inhibitor and heme b_L [21]. However, in the structures containing myxothiazol or similar MOA-type inhibitors, this volume was occupied by the pharmacophoric MOA group

[26,50]. Assuming that QH• formed after the first electron transfer was initially in the same volume as in ES_1 (the site distal from heme b_L), H^+ transfer and rotation of the E295 side-chain would open up the volume proximal to heme b_L when no inhibitor was present. This suggested an additional indirect functional role; by opening up that volume, rotation of E295 might allow movement of $Q^{\bullet-}$ closer to heme b_L, to facilitate transfer of its electron [24,26]. The ~5 Å change in distance would increase the rate constant by >1000-fold, allowing efficient operation at much lower SQ occupancy. The sidechain rotation exposes the backbone >NH of E295 as an H-bond partner for an O-atom of the MOA-group of the inhibitor; in the absence of inhibitor, this would be a potential ligand for SQ in the proximal volume.

Although several publications have raised objections to specific features of the mechanism proposed [31,38,53–56], some support for the proton exit scenario was provided by studies of the role of E295 in Zn-binding and inhibition [52]. In this paper, we have mutated the -PEWY-glutamate to D, G, Q, W, K, and L, and explored the effects on the bifurcated reaction and bypass processes, and their pH dependence compared to wildtype. We have measured the occupancy of SQ in the wildtype and in the mutant E295W, and used these values to estimate the rate constant for oxidation of SQ at the distal domain of the Q_o-site by ferriheme b_L. We address the points criticized, and introduce a kinetic model that illustrates the feasibility of the mobile SQ hypothesis, but leaves unresolved details of how gating to minimize bypass reactions is implemented. We discuss possible mechanisms in terms of a ballet of molecular dancers, with choreography directed by coupled coulombic forces between electron, proton, $Q^{\bullet-}$, heme b_L, and carboxylate groups, all of which have charges in play at different times during the second electron transfer reaction.

2. Materials and methods

2.1. Materials

Biochemical reagents were obtained from commercial sources. Molecular engineering supplies and protocols followed standard conventions [10,57,58]. Horse heart cytochrome c, antimycin-A, and decyl-ubiquinone, were purchased from Sigma and used without further purification. POPC was obtained from Avanti-biolipids. Ascochlorin was a kind gift from Dr. Nobuko Minagawa, Department of Biochemistry, Niigata University of Pharmacy and Applied Life Sciences, Niigata 956-8603, Japan.

2.2. Experimental protocols

2.2.1. Pre-steady state kinetics of quinol oxidation at the Q_o-site

Chromatophores are formed by a pinching off vesicular invaginations of the bacterial cell membrane. Formation of sealed vesicles occurs on cell breakage by mechanical disruption. This traps a periplasmic aqueous volume, including cyt c_2 at a stoichiometry similar to that of bc_1 complex, which is in the membrane. Photochemical reaction centers (RC) are included in the cell membrane, with a stoichiometry about twice that of bc_1 complex, but this can vary with growth conditions. On excitation by actinic light, the RCs generate the substrates (ferricyt c_2 diffusing in the trapped aqueous phase, and QH2 diffusing in the membrane) for the bc_1 complexes, which turn over to regenerate the substrates for the RCs (ferrocyt c_2 and Q). In coupled membranes, turnover generates a proton gradient, with the major component contributed by membrane potential, Δψ. Kinetics of turnover of the photosynthetic chain were measured as previously described, following absorbance changes of the photochemical RC and cytochromes, after actinic flash (~5 μs at half-height) illumination of a dark-adapted suspension of chromatophores under controlled conditions of redox poise, temperature, and pH [3,59–61]. Kinetic traces were recorded at 542, 551, 561, 566, 569 and 575 nm, and specific components convoluted from absorbance changes at the following wavelength differences:

RC oxidized donor (P$^+$), 542 nm; cyt c_1 plus c_2 (cyt c_t), 551–542 nm; heme b_H, 561–569 nm; heme b_L, (566–575 nm)–0.5(heme b_H), with further small corrections for contributions from cyt c_2 and RC dependent on relative stoichiometry. When appropriate, the electrochromic absorbance change of carotenoid pigments that monitor $\Delta\psi$ was measured at 503 nm. In most experiments reported, electrochromic changes were minimized by addition of valinomycin and nigericin to collapse the proton gradient. In experiments to measure the kinetics of $\Delta\psi$ formation, the ionophores were omitted, and the changes at 503 nm were monitored separately.

Activation of RC generates the substrates for the bc_1 complex; when the Q-pool is partially reduced, the time scale for activation of turnover is determined by diffusion of ferricyt c_2 and its oxidation of the high potential chain (cyt c_1 and ISP) with $t_{1/2}$~150 μs, allowing exploration of kinetics in the sub ms range. Because equilibration in both high and low potential chains is more rapid than the rate-limiting first electron transfer, when electron transfer out of the b-heme chain is inhibited by antimycin, the rate of reduction of heme b_H provides a measure of the rate of oxidation of ubiquinol during a single turnover of the Q$_o$-site. By control of redox poise and pH, and with knowledge of the relative stoichiometries of the components, kinetic parameters as a function of substrate concentration, pH, or any other controllable reaction condition, can be readily extracted from the data [3,7,62]. Details of the reaction media, redox mediators, pH buffers, temperature control, and redox poising are given in the figure legends. For kinetic modeling, we used the program Dynafit (Biokin Ltd., Pullman WA) [63].

2.2.2. Molecular engineering, and sample preparation

Rb. sphaeroides strains expressing wildtype and mutant bc_1 complexes were constructed essentially as described in [57]. The expression of the expected mutation was checked by PCR amplification of plasmid DNA from cells used for each chromatophore preparation used experimentally. Chromatophores were harvested from *Rb. sphaeroides* essentially as in [64]. Isolated bc_1 complex was purified in a single step through a His$_6$-tag affinity column as described in [57], followed by extensive dialysis. Concentrations of bc_1 complex were quantified through absorption spectrophotometry by using the dithionite reduced − ferricyanide oxidized difference spectrum at 561–569 nm for heme b_H, using $\varepsilon = 20$ mM^{-1} cm^{-1}. The stoichiometry of subunits was checked by semi-quantitative PAGE analysis.

2.2.3. Preparation of freeze-quenched EPR samples

Isolated bc_1 complex at 20 μM from wildtype or E295W chromatophores was incubated with 200 μM oxidized equine cytochrome c, 20 μM ferricyanide, and 100 μM antimycin A (to inhibit electron transfer from heme b_H, and to prevent formation of SQ at the Q$_i$-site), with and without the Q$_o$-site inhibitor ascochlorin at 80 μM. Absorption spectra confirmed that the bc_1 complex and equine cytochrome c were oxidized prior to mixing (data not shown). To initiate the reaction, the bc_1 complex was mixed with 100 μM decyl-QH$_2$ in a 1:1 volume ratio, to final concentrations of 10 and 50 μM respectively. Both the bc_1 complex and decyl-QH$_2$ were prepared in a buffer of 50 mM MOPS at pH 8.5, 100 mM KCl, 20% glycerol, and 25 μg/ml 1-palmitoyl-2-oleoyl-glycero-3-phosphocholine (POPC). Decyl-QH$_2$ was prepared from decyl-Q using borohydride reduction, and diluted into degassed buffer immediately prior to use. Samples were mixed using a Biologic MPS-20 freeze-quench apparatus, housed in an anaerobic box equipped with gloves to allow manipulations prior to mixing. Before each experiment, the flow-lines were cleared with 250 μl of sample, which was removed by suction. All buffers and samples were degassed under argon for a minimum of 20 min before use in the anaerobic chamber. The reaction was started by mixing 250 μl of each solution, and quenched after 50 ms. Myoglobin-sodium azide control was conducted as in [30], yielding an average freezing time of 35 ms. This, combined with mixing time and calculated time of flight, gave a total dead time of 50 ms. Samples were injected directly into liquid pentane at

−125 °C, and then sealed and stored in liquid nitrogen. Following collection and freezing, the vials containing the frozen samples were thawed in a bath of liquid hexane brought to −60 °C through immersion in liquid nitrogen in a secondary container. Frozen samples were packed into ~8 mm OD EPR tubes using stainless steel rods through a Teflon funnel immersed in hexane at −60 °C. The sample volume in all cases allowed a filling of the EPR tube to a height >2 cm, the maximum height of sample detection. Spin concentration of the SQ was determined using an internal standard (~2 μM Mn^{2+} in final sample), and quantified by double-integration of the EPR spectrum and comparison against a ladder of external Mn^{2+} standards, to compensate for variations in packing density, and fluctuations in detector sensitivity over time. Spectra were measured at 1.0 mW power [30], 5.0 gauss modulation amplitude, 100 kHz modulation frequency, centered at 3320 gauss with a sweep of 160 gauss, effective amplifier gain of 10^4, using microwave frequency ~9.30 GHz, with the value recorded for each measurement to allow calculation of g-values. Traces are the average of 75 scans of 25 s each.

2.2.4. Electron transfer rates for forward and bypass reactions

Protocols were developed for measurement of forward electron transfer and bypass reactions in the pseudo-steady-state, achieved by actinic illumination by a series of closely spaced flashes. Pseudo-steady-state experiments were performed under conditions similar to those for measurement of the single turnover kinetics but with some modifications. For most experiments, reactions were measured under conditions, in which the quinone pool was initially half-reduced (for example, at E_h~90 mV at pH 7.0). The following rates were measured, as illustrated in Figs. 2 and 3:

1) Re-reduction of P$^+$ after a train of 6 saturating flashes spaced at 20 ms (slope (b)). In the absence of an inhibitor in the wildtype (not shown) or in partially inhibited strains (cf. E295D in Fig. 2A), the flux through the electron transfer chain in the pseudo-steady-state includes the bifurcated reaction at the Q$_o$-site of the bc_1 complex, bypass reactions, and back reactions of the RC, and is given by the rate of re-reduction of RC (slope b) plus that for cyt c_t (slope (e)). In the absence of inhibitors in severely crippled mutant strains, or in the presence of antimycin, this flash regime was sufficient to fully oxidize RC, cyt c_2 and cyt c_1, and the rate of re-reduction of RC then measured total flux (Fig. 2B, trace (b)).

2) Rates for the bifurcated reaction were determined from the rate of heme b_H reduction following the first flash in the presence of antimycin (Fig. 2B, trace (a)). If heme b_H was initially oxidized, no reduction of heme b_L was seen after the first flash [3,59], but was delayed until heme b_H was substantially reduced, as expected from the relative E_m values ([59], and see Section 4.3). For severely crippled strains, reduction of heme b_H was only partial during the 20 ms before the next flash, and the initial slope measured during the train was taken (Fig. 3A, trace (a)). When heme b_H was initially partly or completely reduced, the initial rate of reduction of heme b_L could be similarly assayed, starting after the first flash (Fig. 3B, trace (d)), with the total flux through the bifurcated reaction obtained from the sum of initial rates into the two b-hemes.

3) In the presence of antimycin (Figs. 2B and 3), the turnover of the Q$_o$-site becomes inhibited as electrons back-up in the b-heme chain, and the residual electron transfer measured after a train of flashes (trace (b)) is mainly from bypass reactions. In severely crippled mutants, the b-heme chain was not completely reduced after the 6th flash (Fig. 3A, trace (a)), and some residual bifurcated reaction still continued (slope (c)). The rate could be subtracted from the RC re-reduction rate to give the fraction contributed by bypass and back reactions.

4) In the presence of antimycin and myxothiazol, the bifurcated reaction is completely inhibited in all strains, and measurement of RC

re-reduction rates gives residual bypass reactions and back reactions (Fig. 2C).

5) In the pseudo-steady-state after six flashes, the total flux is given by rate of re-reduction of cyt c_t plus that of RC. In wildtype and partially crippled stains like E295D, the relaxation of the chain between flashes is sufficient to allow regeneration of a significant population of reduced cyt c before the flash, and the oxidation of this fraction gives rise to a re-reduction of RC faster than detectable at the time scale and time constant used. This component was ignored, and the rates measured from a point 500 μs after the last flash were considered as representative.

Rates were normalized to the maximal amplitude of the component, measured on activation by multiple flashes in the presence of antimycin (levels indicated by (a), (b), (d) and (e) correspond to amplitudes for heme b_H, RC, heme b_L and cyt c_t, respectively). This could be achieved by poising the redox potential at $E_{h,7} \sim 120$ mV, where the high potential chain was initially fully reduced, the low potential
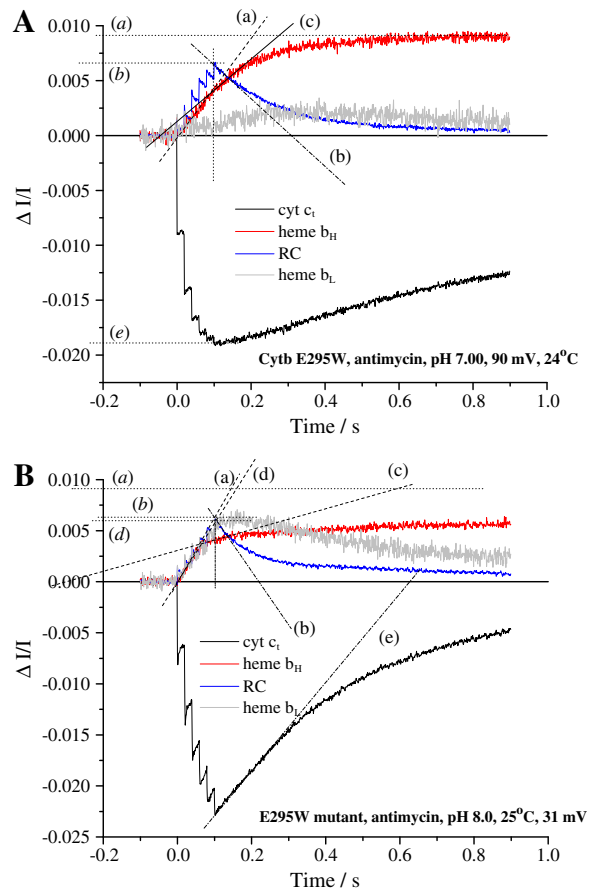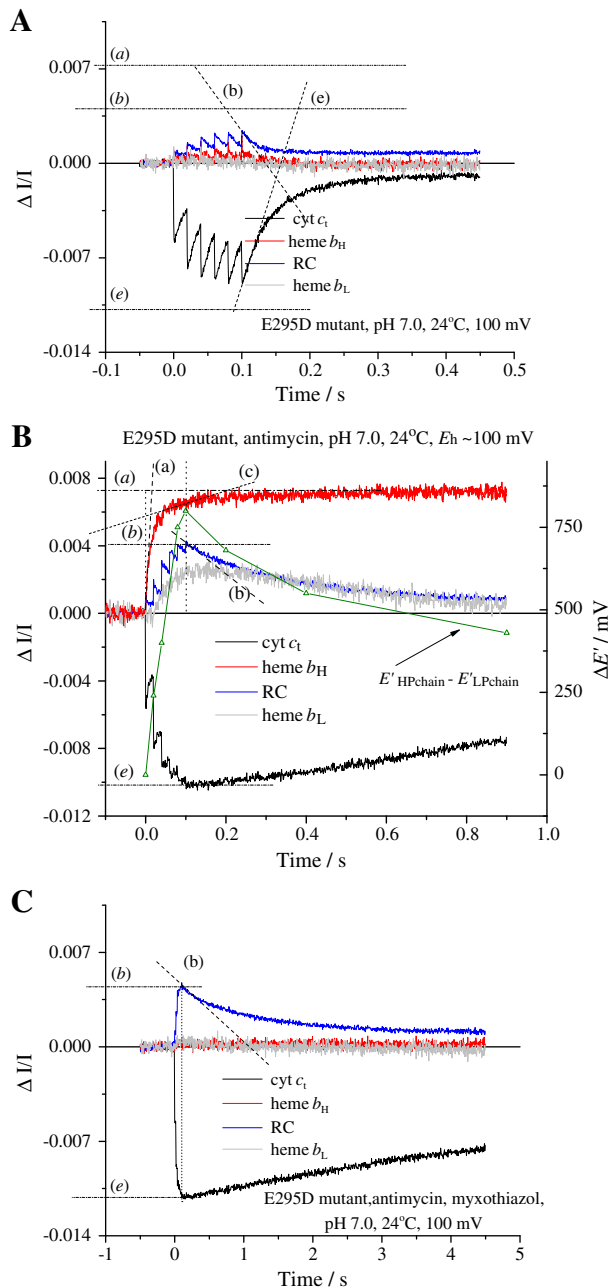

A E295D mutant, antimycin, pH 7.0, 24°C, $E_h \sim 100$ mV

B E295D mutant, antimycin, pH 7.0, 24°C, $E_h \sim 100$ mV

$E'_{HPchain} - E'_{LPchain}$

C E295D mutant, antimycin, myxothiazol, pH 7.0, 24°C, 100 mV

A Cytb E295W, antimycin, pH 7.00, 90 mV, 24°C

B E295W mutant, antimycin, pH 8.0, 25°C, 31 mV

Fig. 3. Partial processes in turnover of the Q₀-site in E295W mutant. A. Kinetics of cytochromes and reaction center at pH 7.0; reaction conditions and labeling of traces as in Fig. 2. B. Kinetics at pH 8.0; reaction conditions as in Fig. 2, but with 50 mM MOPS replaced by 50 mM EPPS.

Fig. 2. Kinetic traces to illustrate protocols used to assay different partial processes. Chromatophores from E295D mutant were suspended in a medium containing 100 mM KCl, 50 mM MOPS buffer at pH 7.0, with mediators to catalyze equilibration of redox centers with the ambient redox potential, E_h, poised at 100 mV. Under these conditions, the ubiquinone pool was ~30% reduced, and the ES_1-complex close to saturated. The b-hemes of the bc_1 complex, and the quinone acceptors of the reaction center (RC) were oxidized, and the high potential chain, and the RC donor, were reduced. The reaction mixture in an anaerobic cuvette was stirred, except during data acquisition. Turnover was initiated by a group of six saturating flashes (~5 μs at half-height), spaced 20 ms apart. Each flash activated >90% of open RCs to generate the substrates of the bc_1 complex. A. Kinetics in the absence of inhibitors; B. kinetics in the presence of antimycin; C. kinetics in the presence of antimycin and myxothiazol. Traces are colored as follows: red, heme b_H reduction ($\Delta A_{561-569}$); black, heme $c_1 + c_2$ (cyt c_t) ($\Delta A_{551-542}$); blue, RC P⁺ (ΔA_{542}); gray, heme b_L ($\Delta A_{566-575}-0.5(\Delta A_{561-569})$ with small additional corrections for P⁺ and cyt c_t depending on relative stoichiometry). The rates of different partial processes were determined from the slopes and amplitudes labeled as follows: (a) initial rate of reduction of heme b_H. In the presence of antimycin, this assays the rate of QH₂ oxidation through the bifurcated reaction. (a) Maximal amplitude of heme b_H absorbance change in the presence of antimycin (1 heme/bc_1 monomer), allowing normalization of rate. (b) Rate of reduction of P⁺, the oxidized RC donor, immediately after the 6th flash, which assays the pseudo-steady state flux from processes leading to relaxation of the system. (b) Maximal amplitude of P⁺ absorbance change to assay total RC, allowing normalization of rate. Since myxothiazol blocks the bifurcated reaction, traces in the presence of myxothiazol assay myxothiazol-insensitive bypass reactions, back-reactions of RC, etc. (c) Rate of the heme b_H reduction (bifurcated reaction) immediately after the 6th flash (to allow correction of bypass rates). This assays the rate in bc_1 complexes in which reduction of heme b_H is incomplete. Subtraction of this rate from that measured in (b) allows assay of bypass reactions. (d) Rate of reduction of heme b_L. At the E_h and pH of this experiment, reduction of heme b_L was delayed until heme b_H was substantially reduced. If heme b_H is initially reduced, reduction of heme b_L is observed after the first flash (see Fig. 3B). (d) Maximal amplitude of heme b_L absorbance change. (e) Rate of reduction of cyt c_t immediately after the 6th flash. This flux must be added to that determined in (b) to obtain the total flux through the high potential chain. (e) Maximal amplitude of cyt c_t absorbance change to allow normalization. See text for further details.

chain oxidized, and the Q-pool 10% reduced. For the bc_1 complex, it was assumed that a monomer contained 1 equiv. each of hemes b_H, b_L, c_1, and ISP. The stoichiometric ratio of RC to bc_1 complex was taken using an extinction coefficient for P^+ measured at 542 nm as 10 mM^{-1} cm^{-1}, and for heme b_H measured at 551–569 nm as 20 mM^{-1} cm^{-1}.

2.2.5. Estimation of turnover from the electrogenic flux

The electrogenic flux associated with turnover of the photosynthetic apparatus was determined by measurement of absorbance changes due to the electrochromic response of carotenoids measured at 503 nm, when induced by a single saturating flash [3,65–73]. The flux of charge across the membrane associated with electron transfer between the Q_o- and Q_i-sites of the bc_1 complex and coupled release and uptake of H^+, was determined by subtraction of the trace measured in the presence of myxothiazol and antimycin (reflecting the RC-linked electrogenic processes) from the change in the absence of inhibitors (reflecting both RC and bc_1 turnover), and normalized to give units $e^-/(bc_1$ complex)/s, using the stoichiometric ratio of RC to bc_1 complex in each strain. The flux assayed at $E_{h,7} \sim 100$ mV matches the rate of heme b_H reduction when the latter is measured in the presence of antimycin [72], and this relationship was assumed at other pH and E_h values.

2.2.6. Estimation of enzyme kinetic coefficients

Values for V_{max} and K_m for QH$_2$ as substrate for the Q_o-site reaction were obtained from linear fits to standard Eadie-Scatchard plots (v/S against v). Redox poise of the ubiquinone pool was varied by changing the ambient redox potential, E_h, and [QH$_2$] was calculated using the standard Nernst–Peters equation, and estimated values for total Q + QH$_2$, and QH$_2$ in the membrane (which varied with redox poise), including QH$_2$ generated in the flash [74]. When the redox poise was measured in situ by reduction of the Q_{pool}, the concentration of both Q and QH$_2$ changed, and values for K_m measured reflect in part the differential binding properties of Q and QH$_2$, as discussed at length in [8,62]. The same set of data could be used to determine apparent affinity of QH$_2$ in formation of the *ES*-complex, with similar caveats [8]. The pH dependence of turnover in the range ≤8.0 was measured from rates of reduction of heme b_H (or b_H plus b_L) in the presence of antimycin. Kinetics of quinol oxidation at pH ≥8.5 were measured from rates of charge transfer across the membrane, assayed via the electrochromic carotenoid band-shift determined from the absorbance change at 503 nm [67,72]. The trace in the presence of myxothiazol (RC uninhibited, no turnover of Q_o-site) was subtracted from that in the absence of inhibitors (both RC and bc_1 complex turning) over to show the fraction of the change due to bc_1 complex turnover.

In strains with the first electron transfer as the limiting step, the apparent pK controlling formation of the *ES*-complex could be determined from the pH dependence of E_m for ISP and the dependence of rate on pH at saturating concentration of QH$_2$ [7,8,13,29,75,76] (see Introduction and Eq. (8)).

3. Results

3.1. General features of kinetics in E295 mutant strains

In the present work, we have extended our earlier investigations [9] to anaerobic conditions at controlled redox poise, pH, etc., in order to further explore the reaction parameters. The mutant strains studied (E295D, L, W, Q, K, and G) all showed substantially inhibited rates for the bifurcated reaction when compared to wildtype. The behavior when assayed under anaerobic conditions was similar to that under aerobic conditions reviewed earlier [9]. The degree of inhibition of the bifurcated reaction was substantially higher than reported in experiments using isolated mitochondrial bc_1 complexes [55], although the antimycin-inhibited rates were similar.

Turnover of the Q_o-site in the wildtype and mutant strains, and rates for bypass reactions, were assayed after a single flash, or in the pseudo-steady state established after 6 consecutive flashes at 20 ms apart as described under Experimental protocols (Section 2.2.4). Rates were measured from the kinetics of absorbance changes of the bc_1 complex and photochemical reaction center (Fig. 3A, B), or from associated electrogenic processes (Fig. 4). In the more severely crippled strains, reduction of heme b_H was still incomplete after the sixth flash (at 100 ms), and continued after illumination because the driving force established by oxidation of the high potential chain continued to sustain the forward reaction. In contrast, the level of reduction of heme b_L leveled off almost immediately, and then declined; this behavior reflects the difference in E_m values of the acceptor hemes (see Section 4.2). At higher pH, heme b_H was partly reduced in equilibrium with the quinone pool at E_h close to E_m [6,59], and in that fraction of centers, reduction of heme b_L started after the first flash (Fig. 3B). Fig. 5 summarizes the results from measurement of initial rates of the bifurcated reaction and myxothiazol-sensitive bypass rates over the range pH 6.0 to 9.0 for the wildtype and mutant strains. All rates measured through the reduction of the b-hemes were corrected for fluxes not associated with the bc_1 complex by subtraction of the residual rate of re-reduction of P^+ after inhibition of the bifurcated reaction by myxothiazol. These residual fluxes came mainly from back-reactions of the reaction center, and minor contributions from mediators, etc., which could not be distinguished from myxothiazol-insensitive short-circuit reactions of the bc_1 complex. The total myxothiazol-insensitive flux represented ~1 e^-/bc_1/s (~0.1% of the steady-state flux in wildtype, or ≤10% of the flux in the presence of antimycin). Note that this myxothiazol insensitive flux is much less significant than reported in mitochondrial complexes ([77], and references therein).

Under aerobic conditions, bypass rates assayed in chromatophores in the presence of antimycin in the pseudo-steady state at pH 7.0 were, for all the E295 mutants, similar to those in the wildtype [9], and were comparable to those previously seen in mitochondrial systems under aerobic conditions [77,78]. When oxygen is present, reduction to superoxide occurs, likely with the Q_o-site SQ as donor [77]. When isolated bc_1 complex was used in these earlier experiments [77], similar rates were seen under anaerobic conditions as long as oxidized cyt c was present as an alternative acceptor. In chromatophores, cyt c_2 is trapped within the enclosed vesicle, so that it can act as electron acceptor, and no addition of c-type cytochrome was needed to observe anaerobic bypass rates using the above protocol. When oxidation of SQ is blocked either by mutation, or by backup of the low potential chain in the presence of antimycin, the pseudo-steady-state flux determined from the rate of reduction of the terminal acceptor, P^+, under anaerobic conditions, includes all bypass reactions involving SQ. Since the rates are similar to those under aerobic conditions, cyt c_2, which is reduced by SO, likely acted as acceptor under both conditions.

A notable feature in all strains was the pattern of equilibria among redox centers following a train of flashes. The strongly inhibited rates for reduction of the low potential chain in mutant strains, associated with the slowed SQ oxidation, allowed us to observe kinetics, and the change in poise of the components of high and low potential chains, and the equilibria of the bifurcated reaction as the driving force increased on successive flashes (Figs. 2B, and 3). Constraints arising from thermodynamic limitations in the Q-cycle ([3,5,44,59,72], and see Section 4.2) were obvious, and provide a basis for calculation of parameters need for estimation of thermodynamic poise of the partial reactions involving SQ (See Section 4.4).

3.2. The pH dependence of the rate of the bifurcated reaction

The kinetic analysis was extended to measurement of the pH dependence of rates of partial processes so as to dissect out the contributions from dissociable species (Figs. 3–5). The pH dependence was tested
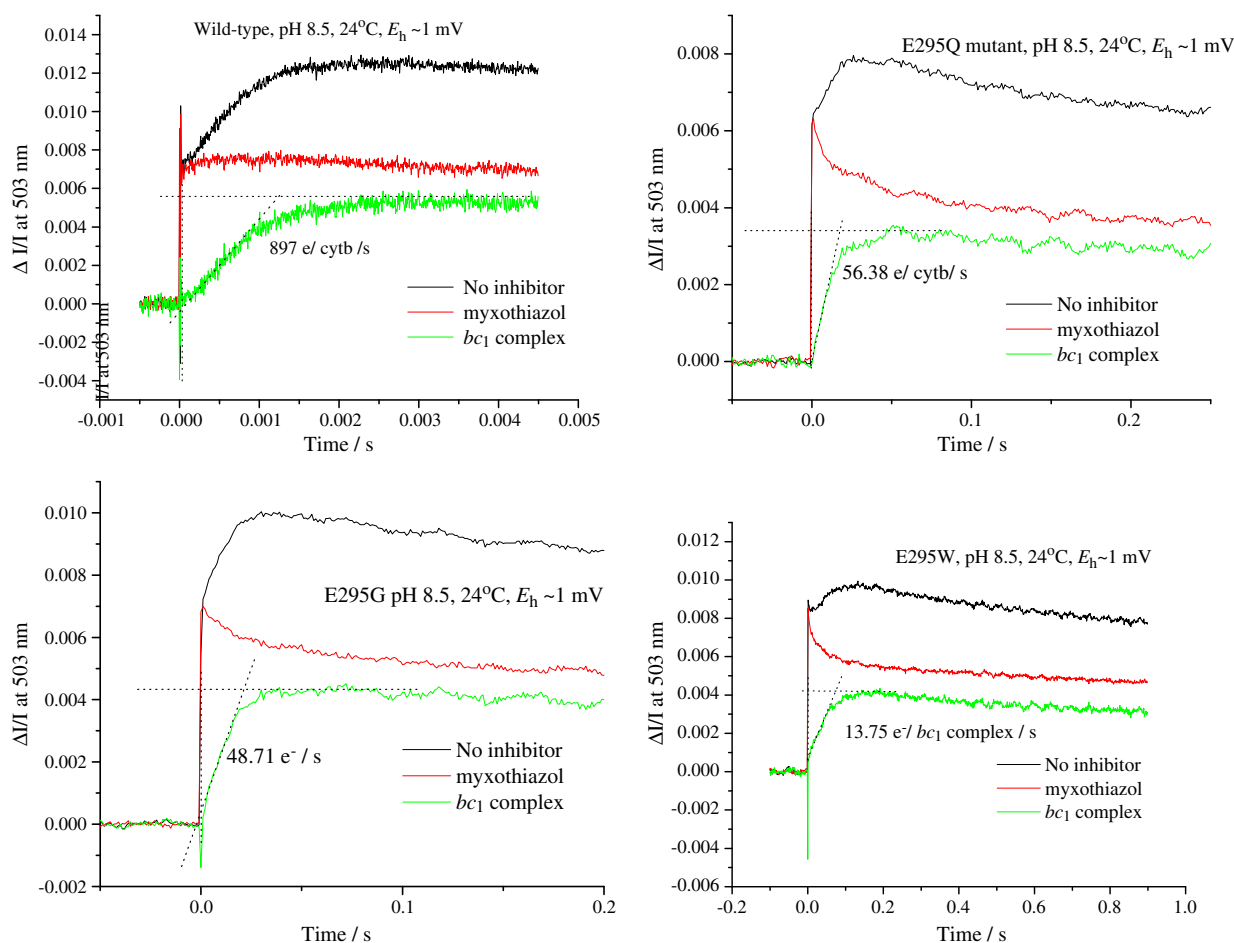
Fig. 4. Q_o-site turnover at high pH assayed through electrogenic reaction of the bc_1 complex. The absorbance change at 503 nm was measured in the absence and presence of myxothiazol, and the difference kinetics used to determine electrogenic processes associated with Q_o-site turnover. The change at 503 nm is the due to electrochromic response of carotenoids to the electric field generated across the membrane by electron transfer from the Q_o- to the Q_i-site, and accompanying H^+ displacements. The change due to reaction center, seen as the only contribution in the presence of myxothiazol, was subtracted.

with E_h poised to keep [QH$_2$] in the quinone pool close to saturating (50% reduced). In the strain with wildtype bc_1 complex, this approach yields a bell-shaped curve for the rate of the bifurcated reaction, fit by two [79] or three [55,80] pK values, the highest of which (pK~9.5)
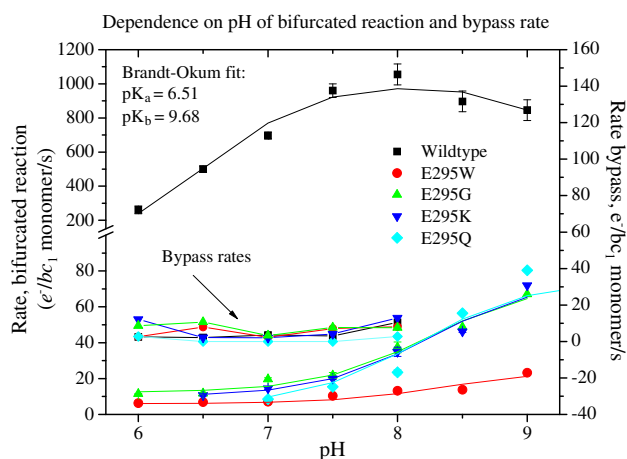

Fig. 5. The dependence of partial processes on pH. Partial processes were assayed as shown in Figs. 2 and 3, under the conditions of Fig. 2, except for the substitution for 50 mM MOPS of the following buffers: pH 6.0 and 6.5, 50 mM MES; pH 7.5, 50 mM HEPES; pH 8.0 or 8.5, 50 mM EPPS; and pH 9.0 or 9.5, 50 mM CHES.

gave the falling edge at high pH. We have interpreted the curve as reflecting contributions of the pK values of ISP to stability of the ES_1-complex [7,8,62]; the rising edge of the bell shape is related to pK_{ox1} (but displaced by the affinity of QH$_2$ for ISP$_{ox}$), and the falling edge to pK_{ox2}, of the histidine ligands to the [2Fe-2S] cluster in the ISP$_{ox}$ state [62,80,81]. This behavior was replaced in the E295 mutant strains tested (E295G, Q, K, and W) by a simpler behavior. There was little pH dependency in the range below pH 7.5, but a strong increase in rate developed over the range above pH 8.0, well described by a single pK~8.5 (Fig. 5). The degree of inhibition compared to the wildtype varied over the range tested. In the lower pH range, where the degree of inhibition was highest, it varied with the rise of the bell-shaped curve, but over the higher range where the bell-shaped curve was falling and the curve for the mutants was rising, the degree of inhibition was smaller. A similar modified pH dependence was previously noted in *Rb. capsulatus* [56] and in mitochondrial complexes [55,82]. The disappearance of the behavior associated with the pK values of ISP$_{ox}$, and the identity of the group conferring the simpler dependence on a single pK, are discussed extensively below (Section 4.6).

3.3. Effects of mutation of Glu-295 on the binding affinity of quinol at the Q_o-site

Using the above protocols, we have measured the fluxes associated with different partial processes as a function of [QH$_2$], varied by changing the ambient redox potential, E_h, and of pH. All mutants tested

showed the acceleration in rate of the bifurcated reaction as [QH₂] increased on reduction of the pool seen in wildtype, as expected from Michaelis–Menten considerations, and followed the same pattern as in wildtype. The change in rate with [QH₂] was analyzed either using conventional approaches to give apparent K_m and V_{max} values [35], or in terms of relative affinity of Q and QH₂ for the Q_o-site ([8], and see Section 4.6), and both parameters could then be determined as a function of pH to look for any dependency of affinities in formation of the ES_1-complex, which might reflect a role for dissociation of essential residues (Fig. 6A,B). Because bypass fluxes are not readily determined from measurement of electrogenic processes, studies of pH dependence were restricted to the range ≤pH 8.

The dependence of rate on degree of reduction of the quinone pool reflects the saturation of the ES_1-complex by QH₂, which in this system is maximal a few hundred μs after generation of the substrates on flash activation. When normalized to [bc_1 complex], the rate gives the fraction of centers in the ES_1 form. The curve of maximal rate as a function of E_h is then a titration of maximal occupancy of the ES_1-complex, [ES_1]. The mid-point potential for formation of ES_1, E_m^{ES}, is shown as a function of pH for the wildtype and E295 mutants in Fig. 6A. The mid-point potentials (taken from the midpoint of the plot of the rate of QH₂ oxidation, estimated from heme b_H reduction, as a function of E_h) were estimated by fitting the titration curve to the Nernst equation for a redox couple with n = 2, appropriate to the Q/QH₂ couple. The apparent association constant, K_{QH2}, for quinol binding on formation of the

ES-complex can then be calculated from $\Delta E_m^{ES-free}$ using Eq. (7) [8]. As seen in Fig. 6A, the ES_1-complex mid-point potentials for the wildtype and E295G, K, W, and Q mutants were not very different over the range pH 6.0–8.0, and followed the slope for titration of quinone free in the pool, displaced by the difference in value between E_m^{ES} and E_m^{free}. From this, the mutations did not have any large effect on the apparent K_{QH2} of the ES-complex. For the E295K and Q mutants, mid-point potentials for the ES-complex were, respectively, slightly higher and lower than the wildtype over this pH range, and complemented the trend seen for K_m. However, within the error of the measurements, the difference from the wildtype was marginal.

Previous kinetic data on E295 mutants showed an apparent K_m for QH₂ up to 2.5-fold higher in E295D and E295G than in the wildtype [24,55,82]. The increase was interpreted as showing a weak contribution from an H-bond between E295 and QH₂ to the binding on formation of ES_1. However, the structures show variation in the configuration of the glutamate with different distal domain inhibitors [1,23,83,84]. In the present work (Fig. 6B), changes in apparent K_m for the E295G, W, K, and Q mutants compared to the wildtype were also small, but in the E295W and K, were in the opposite direction to that previously reported for E295G. Only minor variations were observed over the pH range assayed. In view of the approximations involved in deriving a value for membrane concentration of ubiquinol, and the variation between chromatophore preparations in the stoichiometric parameters involved, we consider the weak variation in values for K_m as a function of pH to be of less significance than the lack of any major pH dependence of this parameter over the range shown.

3.4. SQ formed at the Q_o-site on addition of QH₂ to the oxidized complex

Published values for SQ occupancy of the Q_o-site are conflicting, and no data for E295 mutants has been reported. We have used protocols similar to those reported in [30,32]. Our results are consistent with those of Cape et al. [30]; Fig. 7 shows the SQ signals after correction for the ascochlorin insensitive component (ascochlorin occupies the distal domain of the Q_o-site [84], and is expected to displace all other occupants). The yields of SQ were similar in the wildtype and E295W (though higher in the latter), and at the high end of the range previously reported. Although the subtracted spectra are somewhat noisy, the g-values (2.0061 in the wildtype and 2.0058 in E295W) were, within the accuracy of the noise, similar to those determined in [30], where chemically generate Q·⁻ had g = 2.0056. Our line-widths, however, were both wider (24 in the wildtype and 18 in the E295W), perhaps because of some contaminating background signal that was not subtracted. Our attempts to measure SQ on illumination of chromatophores [32] were inconclusive. When the delay before the measurement was short enough to leave a substantial driving force in the high-potential chain, the EPR signal due to residual P⁺ swamped the SQ signal, as might be expected from the kinetics of decay of the optical signal for P⁺ at 542 nm in Figs. 2 and 3, making accurate determination of occupancy difficult.

3.5. Redox properties of the hemes in wildtype and E295G mutant

The E295G mutant was chosen as an example to test if mutation caused any large changes in the thermodynamic or spectral properties of the b-hemes. The most probable effects would come from loss of the charge of the glutamate side chain, and from changes in packing at the Q_o-site, and this mutant might be expected to show both effects. Thermodynamic characteristics were determined by full-spectrum redox titration over the wavelength range 520–580 nm. Redox potentials of cyt b_L, b_H, and c_1 hemes of the E295G mutant at pH 7.0 ($E_{m.7}$ (heme b_L) = −90 mV; $E_{m.7}$ (heme b_H) = 40 mV; $E_{m.7}$ (heme c_1) = 270 mV; $E_{m.7}$ (cyt b_{150}) = 150 mV (due to SQ:b_H heme interactions (2)), and $E_{m.7}$ (cyt c_2) = 340 mV) were not significantly different from those of wildtype strain, and the spectra were essentially the same. A more
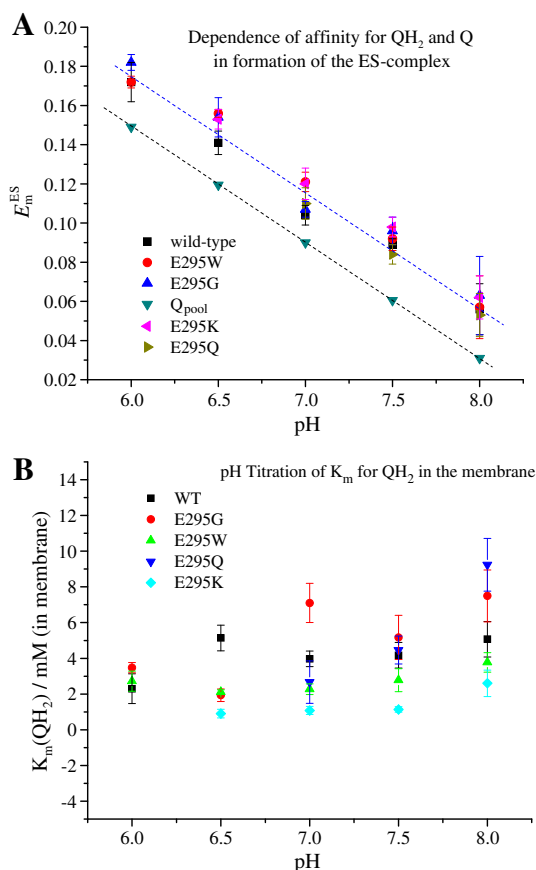

Fig. 6. Dependence on pH of ES_1-complex formation. A. Apparent E_m for formation of the ES_1-complex assayed from the dependence of rate on E_h. The rate of QH₂ oxidation, assayed through the rate of heme b_H reduction in the presence of antimycin, was measured as the quinone pool was reduced by lowering the ambient redox potential, E_h. Since rate is proportional to [ES], the mid-point of the titration give E_m^{ES}. The E_m values for wildtype and all mutants were displaced from that of the pool by ~30 mV, but all showed the same pH dependence. B. Dependence on pH of K_m for QH₂. The same data could be used to calculate K_m values for QH₂ for each strain tested, plotted here as a function of pH (see Materials and methods section).
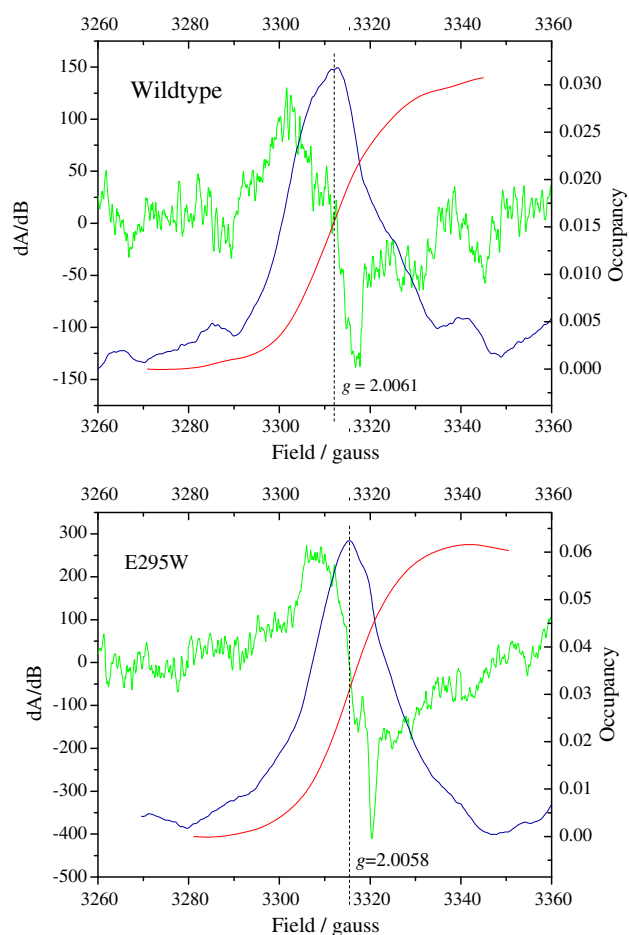
Fig. 7. SQ occupancy at the Q_o-site in wildtype and E295W mutant. The green curve shows the CW-EPR derivative spectrum of the Q_o-site SQ, obtained by subtraction of the signal when ascochlorin was added to the reaction mixture so as to remove components not associated with Q_o-site turnover. The blue curve shows the result of a first integration (to generate the absorbance spectrum), and the red curve a second integration to determine the occupancy, shown by the right-hand scale. Antimycin was present in all experiments to eliminate contributions from the Q_i-site SQ. See Materials and methods section for details.

complete study of a different set of E295 mutants in *Rb. capsulatus* (E295V, K) [56] found no significant change with respect to wildtype in thermodynamic properties determined over a wider pH range (pH 5–10).

4. Discussion

The hypothesis tested was first proposed in a simple and explicit form 13 years ago (24). It had suggested direct roles for E295 in H^+ exit and generation of the $Q^{\bullet-}$ as substrate for the electron transfer step, and an indirect role in facilitating SQ migration in the site to enhance the rate. All were essential, so inhibition of the overall process could have been attributed to inhibition of any step. Critical points supported by our new data can be summarized as follows. E295 certainly plays an important role in oxidation of SQ. The SQ is formed, and its oxidation is inhibited in E295 mutants. At high pH in the antimycin-inhibited wildtype, the SQ was in the dissociated form (30). From the hypothesis, this is the form from which electron transfer occurs. The SQ detected in the wildtype is generated only after heme b_L has become reduced, and therefore unable to act as acceptor of the electron from SQ. As a consequence, no additional information about the electron transfer step could be obtained. However, in the E295W, the

SQ is formed with heme b_L mainly in the oxidized form. In this case, the SQ is likely constrained to the distal domain, and the terms needed to derive *directly* a value for the rate constant for oxidation of the semiquinone from this domain, are the rate of electron transfer to the *b*-heme chain and the occupancy measured. The value determined, 10^3 s^{-1}, is ~1000-fold lower than that calculated on the basis of distance. Our data on binding of Q and QH_2 show essentially the same values in the E295 mutants as in wildtype over the pH range 6–8, suggesting that one feature of the original hypothesis, – weak involvement of E295 in stabilization of the ES_1 complex, – must be revised.

We address the question of dissociation state of SQ in E295W, which requires speculation based on incomplete information. The data show unambiguously that in the more crippled strains the rate of electron transfer increased with an apparent pK~8.5. Since the SQ spectrum is similar in the E295W and wildtype in our experiments, the most economical hypothesis is that the increase reflects an increase in [SQ] due stabilization of the $Q^{\bullet-}$ form as the pH is raised above the pK for this dissociation. If this is so, then the inhibition observed in the more crippled E295 mutants must reflect a stronger effect on the electron transfer than on the proton exit. In the following sections we discuss these points in greater detail.

4.1. Involvement of E295 in different partial processes

Earlier work [24,26] showed that mutation of E295 in *Rb. sphaeroides* to D, Q, and G caused substantial inhibition of the rate of quinol oxidation at the Q_o-site, suggesting a mechanistic involvement in the reaction; resistance to stigmatellin inhibition, and a slight increase in the K_m for QH_2 suggested a role in substrate binding. However, a normal $g_x = 1.80$ EPR signal associated with *EP*-complex between ubiquinone, Q, and ISPH was seen for all the mutants, indicating that binding of Q at the distal site was not perturbed [26,56]. These results supported the suggestion that different domains of the Q_o-site might be of importance in catalysis for the two partial reactions delivering electrons to the high and low potential chains, with the proximal domain and the -PEWY-glutamate involved in the second electron transfer. More recent work [9,36] on these and other E295 mutants has shown that bypass rates in such strains were similar to those seen in the wildtype assayed under antimycin inhibition [9], suggesting that SQ occupancy in the mutants was also similar under these conditions. In the more crippled mutants (Q_o-site turnover ~1% of the wildtype rate), the bypass rates were in the same range as the residual bifurcated reaction assayed through heme b_H reduction, when measured in the neutral pH range. Where tested, these results are confirmed under more rigorous conditions in the present work, but the role in substrate binding is shown to be unimportant.

4.2. The equilibria of the bifurcated reaction

In the wildtype, the Q_o-site reaction is controlled by the thermodynamic parameters of the modified Q-cycle, as seen in the equilibria measured for the reactants involved [3,6]. These reflect three features of the reaction: (i) the rate-limiting first electron transfer; (ii) rapid equilibration in both high and low-potential chains, reflecting the much more rapid rates for other partial processes; and (iii) the equilibrium constant for the bifurcated reaction. Despite the substantial inhibition in the low potential chain, the equilibria between hemes appeared to be controlled by the same values in the E295 mutants. For the oxidation of QH_2, the overall poise is determined by $K_{eq} = \exp(F/RT(E_L^{o'} + E_H^{o'} - 2E_{Q/QH_2}^{o'}))$, where subscripts L and H indicate acceptors in the low and high potential chains [59]. For the first QH_2 oxidized, the acceptors are heme b_H ($E^{o'}$ ~40 mV at pH 7) and (predominantly) ISP_{ox} ($E^{o'}$ ~300 mV), and with Q/QH_2 poised at $E^{o'}$ ~90 mV, K_{eq1} has a value of ~500. For the second QH_2, since the two more favorable acceptors have been consumed, the acceptors are heme

b_L ($E^{o'} - 90$ mV) and (predominantly) heme c_1 ($E^{o'}$ 270 mV), and K_{eq2} then has a value ~ 1.

In chromatophores isolated from strains with wildtype photosynthetic chains grown under standard conditions, there are approximately 2 RC/bc_1 complex [3]. When QH_2 is available in the pool and the antimycin-inhibited reaction is initiated by oxidation of the high potential chain through flash activation of the RC, the kinetics of QH_2 oxidation in the first turnover lead to the reduction of 1 heme b_H per monomer. Little if any reduction of heme b_L is seen because the poise of reactants for the oxidation of the second QH_2 comes up against the low value for K_{eq2}. On subsequent flashes, heme b_L goes reduced as ferroheme b_H accumulates, because the driving force is pumped up by reoxidation of the high potential chain. In the high-potential chain, the oxidizing equivalents from $2P^+$ migrate initially to heme c_1 and ISP, which then get reduced by QH_2 via the bifurcated reaction. The observed rate of reduction of heme c_1 is slower than the rate of heme b_H reduction because the electron from the first turnover re-reduces preferentially the invisible ISP_{ox} [72]. For the same reason, the amplitude of re-reduction of heme c_1 after one turnover of the Q_o-site (assayed ~ 10 ms after the first flash) is partial, because the oxidizing equivalent left is shared between ISP and heme c_1. These properties were of critical importance in allowing a distinction between the modified Q-cycle [3,6,85] and other variants current at the time, including Mitchell's original version [4,5].

A kinetic pattern similar to that on the first flash, – full reduction of heme b_H, and partial reduction (~50%, depending on pH) of heme c_1, – is seen on reduction of isolated oxidized complex by decyl-UQ in the presence of antimycin [31,53,86–88], and is well accounted for by the modified Q-cycle through consideration of the constraints discussed above. However, in experiments with the mitochondrial complex, the behavior has recently been interpreted differently. An ingenious mechanism proposed by Trumpower and colleagues [31,53,86–88] borrows the bifurcated reaction from the Q-cycle, but introduces control by an unspecified mechanism that operates within the dimer to limit Q_o-site activity to only one of the two monomers, giving a half-of-sites functionality. To explain the poise of reactants discussed above, it is then necessary to postulate that the active Q_o-site can access its own high potential chain, but *both* low potential chains through inter-monomer electron transfer at the level of heme b_L. To account for the monotonic reduction of heme b_H observed, the rate of inter-monomer electron transfer would necessarily be more rapid than the rate-limiting step (the first electron transfer), since successive turnovers of the active Q_o-site would reduce first one, then the other heme b_H, and a slower rate for the inter-monomer transfer would lead to separation of the kinetics into distinguishable phases. Furthermore, since both electrons go to heme b_H centers, the equilibrium constants determining poise from this mechanism would differ from those of the Q-cycle; successive turnovers of the active Q_o-site would have heme b_H acceptors with similar E_m, and reactions with similar high equilibrium constants.

The half-of-sites mechanism has received strong support from three studies in which molecular engineering in bacteria had been used to construct systems allowing expression of heterodimeric bc_1 complexes in which differential mutations in the two copies of cyt b enforced inter-monomer electron transfer [53,54,89]. These showed the rapid kinetics seen in the wildtype. In our attempts to reproduce such a heterodimeric expression system, we could measure the rapid kinetics previously interpreted as showing inter-monomer electron transfer, but showed that these were accounted for by cross-over recombination at the DNA level to reconstruct the wildtype homodimer from the heterodimeric construct [90]. We demonstrated that strains in which the heterodimeric constructs enforced an inter-monomer path could not compete with monomeric function. Although this problem had not been discussed in the earlier papers, in subsequent papers [91,92] two groups acknowledged that recombination occurred with high frequency in their systems, and addressed the question

in greater detail. In a more recent paper [93], the rates reported in isolated heterodimeric complexes constructed so as to enforce the inter-monomer path were <10% those measured in similar constructs with the wildtype sequence, – much too slow to be commensurate with the original claims, or with a half-of-sites mechanism. The results previously claimed seem better explained by the same reconstruction of a wildtype operon by the crossover recombination we demonstrated, and by operation of the wildtype monomeric mechanism. Although some slow flux between monomers may well occur, the major flux is clearly carried by a monomeric functionality, and the remaining discussion will be framed in these terms.

4.3. Parameters determining the degree of inhibition at the Q_o-site

In turnover of the Q_o-site, the rate measured in situ in chromatophores (~760 QH_2/bc_1/s at pH 7.0 at 25 °C, with maximal rate ~10^3 s^{-1} at pH 8.0) is that of the limiting reaction, - the first electron transfer from QH_2 to ISP_{ox}. In E295 mutant strains tested, the overall rate decreased by between 13 and 160-fold compared to wildtype (maximal rate for E295D mutant was ~59 s^{-1} at pH 9.0; minimal for E295W mutant was ~4.79 s^{-1} in the range pH 6–7). Although this is a substantial inhibition, representation of the degree of inhibition with respect to turnover in the wildtype can be misleading because the intrinsic rate of the second step in the wildtype is necessarily faster than the limiting rate, and a true measure of inhibition would take account of this. To get a better understanding of the true degree of inhibition, it is necessary to refer the inhibited rates to the operational k_2^{cat} for the 2nd electron transfer under conditions of maximal flux. In principle, k_2^{cat} can be calculated from the observed rate and the occupancy of SQ, using $v = k_2^{cat}$ [SQ·b_L^{ox}], but requires a value for the SQ occupancy. As previously noted [10,72], useful constraints for the wildtype can be established directly from measurements of lag-phases [10,38,72,94,95]; the rate of formation of intermediate states of the second step would be limited by the rate of the first step, and any significant population of such a state would give rise to a delay in electron delivery to the terminal acceptor (heme b_H in antimycin-inhibited chromatophores). Observed lags are in the range 20–30 µs [38,72,95] and give a maximal value for combined occupancy of intermediate states (formation of SQ and ferroheme b_L) as ~0.02 SQ/Q_o-site. In a technical *tour-de*-force, Zhu et al. [38] using rapid-mix freeze-quench and EPR to assay the reactants, failed to detect any SQ attributable to the bifurcated reaction under conditions in which acceptors were available in both chains. Although the authors concluded that no SQ was involved, a more realistic interpretation [10] is that the detection limit was not sufficient to see either SQ, or differences in the ISPH and heme b_L kinetics, in the range expected (see kinetic model below). Cape et al. [30] detected no SQ under aerobic conditions, and since the Zhu et al. [38] work was under such conditions, the failure to detect SQ could alternatively be explained on that basis. However, since their time resolution was sub-millisecond, it seems likely that they would have seen the SQ if it had been formed at measureable occupancy, so their experiment provides a useful constraint. Estimates of occupancy under conditions in which SQ might be expected to accumulate also show some discrepancy. Cape et al. [30] reported values in the range 0.01–0.1 (measured at pH 8 under anaerobic conditions), and Zhang et al. [32] reported values ≤0.01, measured at pH~9, where the SQ stability is expected to be maximal.

The driving force available in the Cape et al. [30] experiments, in which decyl-QH_2 was added to the oxidized complex, should have been limited by thermodynamic constraints intrinsic to the Q-cycle [3] discussed above (Section 4.2). On addition of QH_2 to the oxidized complex, the Q_o-site has to undergo at least one turnover, in a reaction with K_{eq1}~500 (see Section 4.2 for derivation of K_{eq} values), leading to the consumption of the two favorable acceptors, before any SQ could be expected to accumulate. The second turnover would then reach equilibrium with heme b_L and heme c_1 in a reaction with K_{eq2}~1, and in the

absence of additional oxidant would reach a poise leaving heme b_L still largely oxidized [32,53]. The detection of SQ in [30] was therefore somewhat surprising. It seems likely that some additional oxidant was available to pull the reaction further over. Our own data (Fig. 7) show occupancies at the high end of their range under conditions in which an excess of oxidized cyt c was provided, supporting this speculation, and providing firmer data for calculation of values for kinetic parameters.

In the experiments of Zhang et al. [32,37], the bc_1 complex was mutated to remove heme b_H, so that SQ might be expected to form as the second QH_2 was oxidized. The poise of the Q_o-site reaction, measured in chromatophores, was pushed towards products by pumping up the driving force using a group of flashes to re-oxidize the high potential chain while the Q pool was still substantially reduced. The occupancy under these forcing conditions would be expected to be much higher than that in [30], but the measured value was lower. Zhang et al. [32,37] framed their discussion in terms of the stability constant, K_S, for the SQ formation, and estimated a value for K_S in the range 10^{-14} to 10^{-15}. The rationale was to find the difference in poise for the two SQ couples appropriate to the difference in redox potential between the high and low potentials chains under the conditions of experiment, estimated to be ~800 mV from the poise of reactants. The poise can be expressed in terms of $\Delta E'$ values (see below), but they used the relation between the E_m values and stability constant to calculate K_S. Since at maximal yield from disproportionation (the peak of the bell-shaped curve of a redox titration), $[SQ] \approx \sqrt{0.25 K_S}$, one might expect an occupancy in the range $\sim 4 \times 10^{-7}$ under these conditions, much lower than the value they reported, or that from the Cape et al. [30] experiment. Use of K_S in the context of the Q_o-site reaction is confusing because the process in which the SQ is formed and consumed physiologically is not a disproportionation, but is given by Eqs. (2)–(6a, 6b) (see Fig. 1 legend), and it is these equations that should be used. At the low flux of the inhibited systems, the two SQ couples would likely be poised close to equilibrium with the high (highPC) and low (lowPC) potential chains, with $E'_{SQ/QH2} \sim E'_{highPC}$, and $E'_{Q/SQ} \sim E'_{lowPC}$, but through Eqs. (2)–(6a,6b), so that

$$\Delta E'_{SQ/QH2-Q/SQ} = \Delta E'^{o}_{SQ/QH2-Q/SQ} + \frac{RT}{F} \ln \frac{[SQ]^2}{[Q][QH_2]} \qquad (9)$$

might be thought of as the driving force for SQ formation. The $\Delta E'$ values after a group of flashes can be obtained directly from spectrophotometric data like those of Figs. 2 and 3. From simple mass-action considerations, the [SQ] in Eq. (2) would increase as E'_{highPC} increased, and [SQ] in Eq. (3) would increase as E'_{lowPC} decreased, leading to high occupancy at high driving force. (Note however that in the more crippled strains, the low potential chain had not yet reached equilibrium after six flashes (Fig. 3), and the occupancy of SQ would have been higher immediately after the flash than when equilibrium with heme b_L was eventually achieved.) The parameter of interest is the displacement from equilibrium represented by Eq. (9); in effect $\Delta E_{SQ/QH2-Q/SQ}^{'o}$ has the same form as $-\frac{RT}{F} \ln K_S$, but here represents $-\frac{RT}{F} \ln K_{eq}$ for Eq. (9). In deriving values, the driving force ~800 mV (Fig. 2B) immediately after a group of flashes, when most RCs are in the P^+ form, would be appropriate for calculation of occupancy. However, the EPR spectra in [32] showed no significant P^+ in the sample assayed 1–3 s after illumination, so the driving force must have decayed substantially by the time of measurement. From Figs. 2B and 3B (under similar conditions), at 1 s after illumination, P^+ had decayed to <10%, the c-hemes were >70% reduced, and heme b_L >70% oxidized, so the value of ~800 mV is clearly wrong for discussion of their results; a value ~400 mV would seem more appropriate (cf. $\Delta E'$ curve in Fig. 2B). The SQ occupancy expected from Eqs. (2) and (3), would then be much lower than immediately after the last flash, which is in accord with the relatively low occupancy they found. In our own hands, all attempts to measure SQ occupancy of the Q_o-site in

chromatophores under conditions of high driving force (samples frozen <50 ms after illumination by a group of flashes) led to EPR spectra in which the $g \sim 2.005$ region was dominated by P^+, precluding an accurate estimation of SQ. Despite differences in power saturation, we were not able to resolve the two signals satisfactorily (not shown).

4.3.1. The importance of E295 in mechanism

The Q_o-site reactions in Glu-295 mutants were also studied by Osyczka et al. [56] in chromatophores from *Rb. capsulatus*. They measured rates similar to those reported in our earlier study [24] and here. However, they chose to interpret their results in terms of the resilience of the Q_o-site, with glutamate as a nonessential and replaceable component of the reaction. They based their conclusion on the fact that, when expressed in terms of observed rates, the degree of inhibition even in the slowest mutants was never complete, and, in their E295H strain at high pH, approached ~50% of the wildtype rates. Their interpretation of an unimportant role was biased by use of the rate of the limiting first electron transfer as the reference state in determination of the degree of inhibition. As discussed above (Section 4.3), the inhibition is much more dramatic when compared to the rate constant for the second electron transfer, so their choice led them to underestimated the importance of E295.

Wentz et al. [55,96] and Seddiki et al. [82] explored mutations at this site (E272) in the yeast mitochondrial complex. A feature of their studies was an even more modest degree of inhibition in glutamate mutants compared to wildtype. The difference between their observations and ours comes not from the rates observed in the mutant strains, which were similar, but from comparison of these with different rates for the wildtype. In the present work, we measured Q_o-site turnover ($\sim 10^3 \text{ s}^{-1}$ at pH 8) (Fig. 5) with the complex in its native membrane and the native Q-10 reacting from the lipid phase. In the studies with the yeast complex, the activity in wildtype was ~10-fold slower (75 s^{-1} [82], 52 s^{-1} [55], or 120 s^{-1} [95]) when assayed in the isolated protein through steady-state cyt c reductase activity using decyl-QH_2 as substrate. Even slower steady-state rates have been reported in bacterial complexes when determined using the detergent solubilized enzyme in a similar assay (cf. [54,97,98]). However, when a single turnover of the bacterial enzyme was measured in similar preparations through photoactivation of the high potential chain, rates of heme b_H reduction and heme c_1 re-reduction were comparable to those seen in situ [95], showing that the pathways for Q_o-site catalysis within the enzyme were not impaired by detergent isolation. Likely these rapid rates reflected the single turnover using bound $(Q-2)H_2$, initially present at concentration saturating occupancy of the ES_1-complex. Possibly, the steady-state flux was limited by the rate of exchange of decyl-Q (or Q-2) couples, partitioned between separate micellar phases in the detergent solubilized mix.

As discussed at length above, any observable inhibition likely represents a loss of activity in the *second* step, which then becomes the limiting process, reflecting minimally a 100-fold inhibition with respect to the effective k_2^{cat}. The inhibition is always substantial and reflects an important role of Glu-295 in catalysis. The fact that inhibition is never complete is intrinsic to the mechanism proposed, and reflects bypass reactions and the residual rate of the bifurcated reaction on accumulation of SQ.

4.4. Semiquinone occupancy at the Q_o-site under forward and under forcing conditions

In our experiments under conditions similar to those of Cape et al. [30], the occupancy was at the higher end of the range they reported. The value expected under normal forward chemistry (with acceptors available in both chains) would, of course, be much lower than under these forcing conditions and likely too low for direct measurement (cf. [32]). In the following discussion we will assume initially an occupancy of 0.01SQ/Q_o-site, consistent with the limits from kinetic data,

and then discuss plausible ranges under uninhibited and under forcing conditions. We will then use the SQ occupancy we measured to estimate an empirical value for the rate constant for oxidation of SQ in the distal domain by heme b_L, and from this derive other thermodynamic and kinetic parameters.

For electron transfer using parameters $\lambda = 0.7$ V, and $\Delta G^{o'} = -0.1$ V, assuming a Marcus treatment of the Arrhenius term [10,99], and the dependence of intrinsic rate constant on distance [100], the 11.5 Å for an edge-to-edge distance from an occupant of the distal domain to heme b_L gives a value for k_{2d}^{cat} of ~10^6 s^{-1}, and for the 6.5 Å from the proximal position gives k_{2p}^{cat}~10^9 s^{-1}, values similar to those used in previous discussions [7,9,44,101,102]. How reasonable are these values? The maximal rate measured in uninhibited chromatophores (~10^3 e$^-$/bc_1/s^{-1} at pH 8), is determined by the rate constant for the first electron transfer with a saturated ES_1-complex (occupancy ~1). To match this rate for the second electron transfer using occupancy of 0.01, a minimal value for k_2^{cat} would have to be in the range 10^5 s^{-1}, compatible with the value derived from distance. Given the uncertainty of occupancy values from earlier experiments, a simple mechanism in which the SQ could donate electrons to heme b_L from the distal domain could not be excluded [44]. However, three factors make this naïve scenario questionable: (i) the reaction is certainly not a simple electron transfer, (ii) the occupancy under uninhibited flux must be much lower than the value under inhibited conditions, so likely the value used in the example above is an overestimate, and (iii) the intrinsic rate of removal of SQ would have to substantially exceed the rate of generation in order to account for the pattern of dependence on driving force in mutants; the full effect from changes in E_m for ISP [62] is as expected from Marcus theory if the first electron transfer is limiting, and the lack of any consistent effect from changes in E_m for heme b_L on the overall rate (for example, enhanced rate when E_m of heme b_L is raised) is consistent with a much faster intrinsic rate for the second electron transfer [103]. Assuming a factor of ten for each of these last two points, we would need a value $k_2^{cat} > 10^7$ s^{-1}, raising the question of consistency with mechanisms based on electron transfer from the distal domain using the value suggested by the distance.

When similar considerations are applied to the E295 mutants, the naïve treatment of rate constant becomes more obviously flawed. An important technical point to note is that, because rates in the E295 mutants are so slow, they can be measured at a time, < 50 ms, corresponding to that at which SQ is sampled. With $t_{½}$ ~ 100 ms, most centers would still have heme b_L oxidized, so that an empirical rate constant for the bifurcated reaction could be determined directly. For the bulky sidechains (E295Q and E295W), the SQ would likely be constrained to the distal domain, and SQ occupancy would likely approach the maximal value allowed by the equilibrium constant for the first electron transfer, K_1, and by driving force. Measurement of occupancy for SQ in E295W therefore provides, for the first time, an empirical value for the rate constant of the bifurcated reaction. Using values measured at pH ~8.5, and by substitution in $v = k_2([SQ \cdot b_L^{ox}])$ we get a value for k_{2d}^{cat} of ~10^3 s^{-1}, which is 3-orders of magnitude smaller than the value calculated from distance. We use approximate values ([SQ] in the range 0.05–0.1/Q_o-site, rate ~60 e$^-$/s/bc_1 seen with E295Q in Fig. 4) because we recognize that occupancies might vary in different strains, and because in E295W the bulk of the tryptophan might lead to artificial displacements in the site leading to lower rates than for more native side chains. As a consequence, the rate constant calculated is higher than if we had used rates derived from E295W data.

One clear conclusion is that the rate constant calculated from distance is inappropriate for the reaction under these conditions. Factors other than distance must come into play. Given the complexity of the second electron transfer step, it is perhaps not surprising that other parameters might modulate the rate. It will also be obvious that if the value for k_{2d}^{cat} (~10^3 s^{-1} from the distal domain) is also appropriate in wildtype, and SQ was restricted to the distal domain, then no occupancy consistent with the measured lag phases could also be

consistent with the observed uninhibited rate. Use of the same rate constant from the distal domain in the wildtype and E295 mutants is the most economical hypothesis, and is supported by the kinetic model (Section 4.9), and by the fact that bypass rates are similar in all strains, but the impact of this conclusion depends on whether or not the reactants are the same, and hence on the dissociation state of SQ, discussed further below.

While the rate constant calculated from distance is clearly inappropriate for transfer from the distal domain, if SQ were to move close to heme b_L, the reaction might be a simple electron transfer, and the value expected from distance (k_{2p}^{cat}~10^9 s^{-1} for 6.5 Å) would then be appropriate, representing a maximal operational value. Any observable inhibition of the bifurcated reaction (as in the E295 mutants) must indicate a rate less than the limiting first step (~10^3 s^{-1}), and (since occupancy is low) a substantial inhibition, but a realistic kinetic model and justifiable constraints are needed to estimate a degree of inhibition with respect to an operational k_2^{cat}.

Knowledge of the occupancy for SQ also allows us to use the equilibria in the two chains to provide an estimate of the potentials of the two couples, and of equilibrium constants for the two steps of the bifurcated reaction. Recognizing that in the inhibited system, after six flashes the reactions in the two chains come close to equilibrium, and using $E'_{SQ/QH2} \sim E'_{highPC}$, $E'_{Q/SQ} \sim E'_{lowPC}$, and

$$\Delta G'_{overal} = -F\left\{\left(E'_{ISP} + E'_{heme b_L}\right) - 2E'_{Q/QH2}\right\} \quad (10)$$

for the Q_o-site reaction, taking values from the experimental E_h and the kinetic traces, and $E'_{Q/QH2} \sim 90$ mV (for the Q-pool), we get $E'_{SQ/QH2} \sim 500$ mV, and $E'_{Q/SQ} \sim -320$ mV. Then, using $E' = E_m + 59 \log_{10} \dfrac{SQ}{QH_2}$ (with [SQ] ~0.06), we get $E_{m\ SQ/QH2} \sim 570$ mV, and an equilibrium constant for the first electron transfer, $K_1 \sim 10^{-4.5} \sim 0.00003$. With the Q-pool as reference, $E_{m\ Q/SQ}$ is then ~-390 mV, $K_2 \sim 10^5$, and the overall equilibrium constant, $K_{overall} \sim 3.5$, — the same value as obtained directly from $\Delta G'o$ on substitution of E_m values in Eq. (10). Formation of ES_1 showed a midpoint, E_m^{ES}, displaced from that of the pool by ~30 mV (Fig. 6A), so discussion with respect to that as starting state (the configuration used in the kinetic model of Section 4.9), requires consideration of the ~10-fold displacement in favor of QH_2 binding indicated by this ΔE_m. These values are used in the kinetic model discussed below (Section 4.9).

4.5. Involvement of Glu-295 in transfer of the second electron and proton

Since, from the discussion above, the rate constant from the distal domain would give a rate > 100 times too slow, movement of SQ to allow migration closer to heme b_L, facilitated by rotational displacement of the E295 sidechain, becomes an attractive possibility [24]. This opens the question of whether the inhibition observed involves the direct role in proton exit, or the indirect role in facilitation of electron transfer. What conclusions about the behavior can be drawn from particular mutants? Several properties of the glutamate side chain might be expected to be of importance, - the acidic nature, polarity, length, bulk, mobility, etc. The role in proton exit has been supported by studies of the role of E295 in Zn-inhibition, which likely involves participation of groups that otherwise stabilize the water chain [52]. However, exploration of this role, and of any role E295 may play in gating [9,10], must be approached indirectly, since no such intermediate states have been directly observed. The E295D mutant has an acidic side chain, shorter by 1 –CH_2 than the wildtype, and shows the least perturbation of behavior. E295G is next in line, and has no side-chain. All the other mutants are more severely crippled, including E295Q, which shares all characteristics of glutamate except the acidic nature. From the differences, we can infer that the acidic property is most important, that the length of the native side chain is required for maximal rate, and that, absent the carboxylate

function, a bulky side chain introduces more severe constraints than a small one. We discuss these roles more fully in the following paragraphs.

4.6. Contribution of Glu-295 to the affinity of QH₂ at the Q₀-site

Although mutation of Glu-295 had a dramatic effect on the overall rate of QH₂ oxidation, it is unlikely that the inhibition had any major direct effect on rate constants for the first electron transfer. We would expect to see an effect on K_m if glutamate stabilized the ES_1-complex. In stigmatellin-containing structures, the E295 carboxylate forms a H-bond with an –OH group of the inhibitor, and this feature was incorporated into early models of the ES_1-complex, leading to an expectation that E295 would contribute to the affinity of the site for QH₂. Indeed, in earlier work, a ~2-fold increase in K_m was measured, in the expected direction [24]. In the present work, the changes in binding affinity of QH₂ in the Glu-295 mutants compared to wildtype were also small, but there was no consistent pattern to the sign of change; − K_m increased in some strains but decreased in others. From this it seems clear that, in agreement with [56,82], the contribution, if any, of the H-bond to QH₂ affinity is too small to explain any major fraction of the substantial inhibition observed in mutants.

Since the first electron transfer is endergonic, the inhibition in mutants could be readily explained by a reduced rate of removal of the intermediate SQ. This second step can be dissected into two main components, - electron transfer and proton transfer. In order to participate in proton transfer, the E295 side chain would have to be in the carboxylate form to act as H⁺ acceptor from QH•. The consistency of this assumed polarity would depend on the pK values of QH• and E295. The values in solution might be similar, but pK values in the protein can vary widely from those measured in an aqueous environment. The lack of any major effect of pH on K_m suggests that neither the glutamate nor the quinol has a pK that affects ES_1-complex formation in the pH range (6 to 8) tested. Since the dependence on pH of E_m^{ES} tracked that of E_m^{Q-pool}, we can also conclude that there was no marked pH dependence on K_{QH2}, or on relative affinities of Q and QH₂ when ISP₀ₓ is the partner. It was previously noted in studies of E295 mutations in *Rb. capsulatus* [56] that in formation of the $g_x = 1.80$ complex, neither the affinity of Q or QH₂ (measured from the E_m for the change in EPR line intensity of the $g_x = 1.80$ complex on reduction of the Q-pool), nor the apparent E_m of ISP, were modified in the mutants. However, the $g_x = 1.80$ complex is an *EP*-complex, in which the participating species are Q and ISPH [26,47], and is relevant to ES_1 only insofar as these states are present before flash-excitation (likely in ~60% of centers at $E_{h,7} \sim 100$ mV [72]). The $g_x = 1.80$ complex is of no relevance to the ES_2 complex in which QH• is the substrate; none of these results precludes a role for E295 in liganding the QH• state.

The question might be raised as to why in the mutant strains we observe a dependence of rate on substrate concentration for QH₂, but not for ISP₀ₓ, since both are required for formation of the ES_1-complex. The answer lies in how the two values are measured. For each value of E_m^{ES}, the dependence of formation of ES_1 on [QH₂] was measured at fixed pH. Since the second electron transfer depends on the product of the first, that dependence is reflected in the rate measured, although the second step is limiting. In contrast, dependence of rate on [ISP₀ₓ] is assayed by changing pH, and the weak contribution from the first electron transfer in the low pH range is swamped by the much larger pH dependence of the 2nd electron transfer in the high pH range.

4.7. The role of E295 in the bifurcated reaction, and the pH dependence in mutant strains

The preceding discussion was framed without reference to the dissociation state of SQ, the parameters calculated all pertain to the general case, and would be valid for a neutral or anionic SQ. In this section we discuss the dissociation state of the SQ species observed.

4.7.1. Interpretation of the pH dependence of the bifurcated reaction in E295 mutants

As noted earlier (Sections 1.2 and 3.2), the bell-shaped Brandt–Okun [79] pH profile of the wildtype Q₀-site reaction can be well accounted for in the range below pH 8 by the involvement of the imidazolate form of His-152 of ISP₀ₓ, and the role of the pK₀ₓ₁ of this group in formation of the *ES*-complex [8,27,62,104]. The pK values determined from redox behavior in the isolated ISP, pK₀ₓ₁ ~7.6, pK₀ₓ₂~9.6, can be assigned unambiguously to His-152 and His-131 respectively [28,105]. The value for the pK₍app₎ determined experimentally tracks the value of pK₀ₓ₁ on mutation of ISP, and since His-152 is the residue involved in H-bond interaction with QH₂, we can take this as demonstrating a direct relationship between pK₍app₎ and pK₀ₓ₁, and assign the difference in value (ΔpK~1.1) to the free-energy contributed by this interaction to formation of the ES_1-complex [8] (see Section 1.2 and Eq. (8) for derivation of ΔpK).

Wentz et al. [55] studied the pH dependence in the E272D and Q mutants in the yeast complex, and observed loss of a component corresponding to a pK~6.2 from a three pK fit [80] (the slope of the wildtype curve was shifted to lower pH than in other studies). They interpreted loss of the pK at ~6.2 as reflecting replacement of the glutamate. However, the direct association of pK₍app₎ with His-152 of ISP₀ₓ makes this explanation implausible [62]. Osyczka et al. [56] also determined the pH dependence of rate in the *Rb. capsulatus* complex, and for strains common to the two studies, results were similar to ours. However, the pH dependence in their less inhibited strains showed a less dramatic shift in the range below pH 7.5. No simple interpretation or firm conclusions from their results was offered [56].

In our more severely inhibited E295 mutants, the Brandt-Okun behavior was lost, and the pH dependence was relatively weak over the range pH 6–7.5. Instead, the pH profile showed a steep increase in rate over the range pH 8–9, where the wildtype shows a decrease in activity. The pK for the increased rate is in the range ~8.5 ± 0.3 for the four strains tested. Note that the protocol for measurement means that this pK reflects only the bifurcated reaction. Since the pK~6.5 in wildtype is well explained by the involvement of ISP His-152 in formation of the ES_1 complex, the loss of the pK~6.5 cannot by attributed to loss of E295 [55]. Rather, it is likely due to loss of the controlling role for the first electron transfer, and its replacement by a limitation in the second electron transfer in the E295 mutants. The ionizing group revealed must be from some partial process of the second electron transfer step, but could include either the proton exit or the electron transfer pathway or both. The most obvious candidate for the dissociable species is the substrate semiquinone, undergoing dissociation from the neutral to the anionic form. Cape et al. [30] showed that the SQ detected in wildtype was in the anionic form. This was based on comparison of line width and g-value of the Q₀-site SQ to species generated chemically, and on ENDOR measurements of proton couplings. Our own spectra for SQ in E295W showed a similar g-value, but the quality of the signal means that we cannot claim strong support for an anionic species on this basis alone, and we have not yet generated samples appropriate for high resolution studies which would provide a definitive assignment. Other possible candidates are protein side chains, but the structures show E295 (lost in the mutants), and His-152 (the ligand from ISP) as the only dissociable groups within 7 Å of the stigmatellin ring (in PDB ID: 2qjy). E295 mutations with Glu replaced by Gly, Trp, or Gln do not have pKs, and for Lys the pK would likely be higher, but all showed titrations with the same pK ~8.5. Of the residues in the Zn-binding site in *Rhodobacter* bc_1 complexes [52], suggested to be associated with proton exit, only E295 could directly affect SQ by dissociation, since His-276 at 7.98 Å, Asp-278 at 10.11 Å, are too distant to act as ligands, and Asn-279 is not dissociable. Although we cannot rule out indirect effects from this set, the site is not conserved between mitochondrial and bacterial complexes. Since the profile of pH dependence in the more crippled strains was similar between yeast bc_1 and the bacterial

complex, it seems unlikely that residues peculiar to the bacteria site are responsible for the $pK \sim 8.5$.

4.7.2. The pathway inhibited in E295 mutants

In experiments with the isolated complex, a significant driving force would be attained within 50 ms on mixing with QH_2. In the kinetic experiments using 6-flash groups, the full driving force ($\Delta E' \sim 800$ mV) is established by 100 ms; equilibration of the high-potential chain with SQ/QH_2 couple should occur on this timescale in the E295 mutants. However, the rate of electron flow was still markedly inhibited, despite the high occupancy of SQ. The inhibition is clearly after formation of SQ, and before electron transfer to heme b_L. Although electrons and protons likely follow separate pathways in the overall process, both species have to be removed for net forward flux, and the two fluxes are likely closely coupled. In which pathway is the inhibition occurring in the E295 mutants? In the mechanism proposed for the wildtype, $Q^{\bullet-}$ is the immediate electron donor, and the species detected in [30] was unambiguously this anionic form. In both wildtype and E295W, the driving force in our experiments was initially the same, and generated a similar occupancy. The higher value in E295W could be trivially explained, as discussed in Section 4.9.1 (see the model kinetics in Fig. 9F), using the same equilibrium constant. In that case, the same thermodynamic parameters would have to pertain to the SQ species (see Section 4.8.2 for further discussion). If the species in E295W is also anionic, then the increase in rate at high pH would be simply explained by the increase in occupancy of this form, and the electron transfer rate would not be limited by deprotonation. Inhibition would then have to be attributed to some other process after formation of $Q^{\bullet-}$. How does this relate to the mechanism in wildtype? The SQ is likely formed in the distal domain and the anionic form is the substrate for electron transfer, so, if SQ was anionic in both cases, the rate constant from the distal domain derived from the inhibited rate in mutants would be appropriate for electron transfer to heme b_L from this domain in wildtype. If so, some additional process has then to be invoked to account for the *uninhibited* flux (at much lower SQ occupancy) in the wildtype. Movement of SQ in the site [24] seems the most natural candidate, with inhibition of movement as the consequence of mutation. We favor this as the most parsimonious explanation. However, we recognize that it must remain hypothetical until the pK values and dissociation state of the SQ species in all the E295 mutants is resolved.

If the SQ is anionic, this need not imply that deprotonation and proton exit were uninhibited. These processes could be slowed by orders of magnitude, and still be fast enough to populate the $Q^{\bullet-}$ state so long as the rate of electron transfer was slower still. However, catalysis of deprotonation by E295 in the wildtype would be replaced in the mutants by a simpler pH dependence and proton equilibration with the external aqueous phase by less efficient pathways. If SQ movement was only partially inhibited in other E295 mutants, proton exit could be the controlling process. In the hypothesis, E295 has functions in both pathways, inhibition of either would slow both, and the degree to which either path was inhibited could be similar.

4.8. Scenarios for gating

Osyczka at al. [44] had argued persuasively that the Q-cycle would be decoupled unless some mechanism prevented short circuit reactions from occurring, but suggested that "only by eliminating the SQ intermediate in a concerted reaction, or by introducing double gating of a SQ intermediate…" could the mechanism be saved. Since the involvement of SQ seemed well established, we have preferred the second option.

4.8.1. Empirical rate constants for bypass processes

Muller et al. [77] suggested plausible bypass reactions and subsequent discussion (cf. [9,44]) has been framed in this context. Our determination of SQ occupancy allows calculation of empirical values for rate constants for these bypass reactions. The main reactions of interest are:

(i) electron transfer from SQ to O_2 or the high potential chain; and (ii) the reduction of SQ by heme b_L^- [77] (reduction of Q by the reversal of the normal forward reaction is not a bypass process). Since in the more crippled E295 mutants, rates for bypass reactions are similar to those for the bifurcated reaction, a value can be derived from the parameters determined above: $v_{HP} = k_{HP}$ [SQ]·[2nd reactant] ~5 s^{-1}, and $v_{LP} = k_{LP}[SQ \cdot b_L^-]$ ~5 s^{-1}. For (i), under aerobic conditions, since the rate of SO formation saturates at $\sim 10^{-4}$ M O_2 [77], the value for k_{HP} would be in the range $\sim 10^7$ M^{-1} s^{-1}. In the absence of O_2, the local activity of the second reactant (ISP$_{ox}$ in an appropriate configuration), is unknown, so speculation must be limited. For (ii) with heme b_L fully reduced, k_{LP}[SQ] would have to be $\sim 10^2$ s^{-1}, with $k_{LP} \sim 10^3$ s^{-1} at [SQ] of 0.1, much lower than the value from distance assumed in the stochastic models (101,102,121). Reduction of either QH• or $Q^{\bullet-}$ to QH_2 would necessitate uptake of one or two H^+, so it is clearly not a simple electron transfer, and it is unlikely that the distance dependent value for k_{LP} would be appropriate.

4.8.2. Gating mechanisms

We suggested that bypass reactions of type (ii) could be averted by minimizing electron transfer between SQ and heme b_L when the heme is reduced, and we proposed a coulombic mechanism to account for gating [9]. Likely, the electron and proton follow different paths, and $Q^{\bullet-}$, the E295 and heme propionate carboxylates, and the heme itself, all change their charge at different stages of the reaction, so they are all coulombic 'dancers' in this ballet. Given the pH dependence of E_m for heme b_L, the oxidation of $QH^{\bullet}$ by heme b_L would overall be a neutral process. Since charge is conserved, separation of paths for electron and proton transfer present possibilities for electrostatic interaction during oxidation of QH•, and offer considerable scope for speculation. Any such mechanism must depend on details of the electrostatic profile around the reactants, and on the changes in charge of species during the overall electron/proton transfer reaction. The ferriheme b_L carries a formal positive charge, which if uncompensated would provide an electrostatic attractant for the mobile $Q^{\bullet-}$ postulated in our mechanism, thereby facilitating movement to the proximal domain. In this case, the ferroheme might be neutral, and the coulombic repulsion of the gating mechanism previously suggested [9] would then be inappropriate. On the other hand, the low potential of heme b_L suggests a local environment in which the protein provides a compensating negative field. If this were so, the ferriheme state might be neutral, and the mechanism previously discussed [9] would remain attractive. However, although a single electron charge is transferred, it could well be to an oxidized heme of partial charge δ^+, resulting in a charge $(1-\delta)^-$ after transfer of the electron; then perhaps the most attractive scenario would involve a mix of these two mechanisms, and both attractive and repulsive effects would come into play at different times during the evolution of the process. The scheme in Fig. 8 sketches such a scenario (see legend for explanation).

4.8.3. Proton exit pathways

For gating mechanisms associated with coulombic interactions between the charged participants, all the dancers have to be considered. In this context, the relative pK values governing the proton pathway between QH•, E295, and the aqueous phase must also be considered. If the pK at ~8.5 measured in the E295 mutants does reflect dissociation of QH•, then two general cases might be argued:

(i) The pK ~8.5 measured in the more crippled E295 mutants might reflect dissociation of QH• appropriate only to the case in which the carboxylate function is missing. If this were the case, the working pK of QH• in the wildtype might be much lower, with a favorable gradient for H^+ transfer along a pathway in which QH• and E295 have pK values close to those in aqueous environments. The fact that the species measured by Cape et al. [30] in wildtype at pH 8.0 was the anionic form would favor this interpretation.
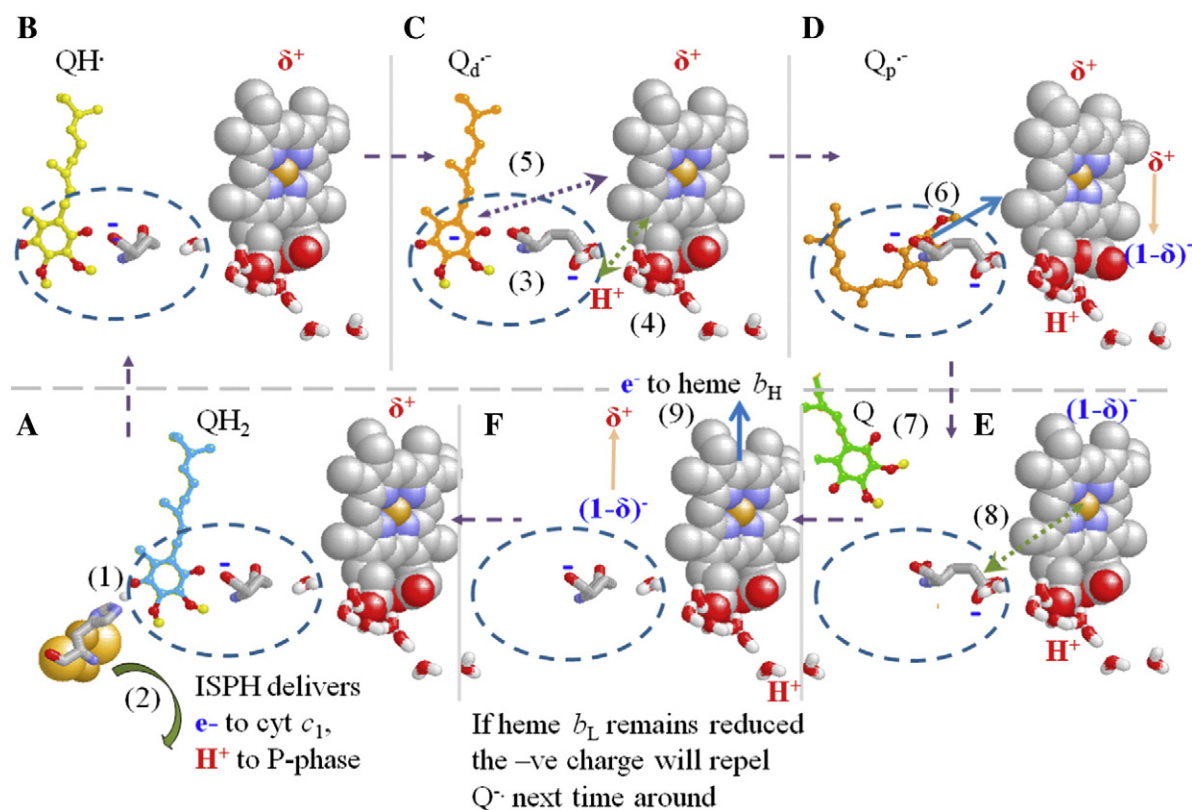
Fig. 8. Scheme to show possible mechanistic features of the Q_o-site ballet. a. Before the 1st electron transfer, the ES_1-complex forms in the distal volume of the Q_o-site, stabilized by a strong H-bond to His-161 of ISP_{ox}. E295 may H-bond weakly to QH_2. Heme b_L is in the oxidized form (with local field of δ^+ charge). An electron and H^+ are delivered to ISP_{ox} to form ISPH (1). Immediately after the 1st electron transfer, the ISPH rotates away (2) to deliver its electron to cyt c_1 and release the H^+ to the P-phase. b. This leaves the neutral SQ (QH•), H-bonded to E295 carboxylate in the ES_2-complex. Heme b_L is still oxidized, and available as acceptor for the electron from QH• (or $Q^{\bullet-}$), but the low occupancy, and low value for k_{2d} ($\sim10^3$ s^{-1}) means the rate is slow. c. The H^+ is transferred to the E295 carboxylate, to form the SQ anion ($Q^{\bullet-}$), and E295 (3), now in carboxylic form, rotates to open up the proximal volume. The sidechain makes a H-bond to the water chain leading to the P-side aqueous phase. The δ^+ field around heme b_L lowers the pK, allowing release of the H^+ (4), which transfers down the water chain, leaving E295 in the carboxylate form. The δ^+ field also attracts $Q^{\bullet-}$ (5), which migrates closer to heme b_L, increasing the rate constant ($k_{2p}\sim10^9$ s^{-1}). d. The electron from $Q^{\bullet-}$ transfers rapidly to heme b_L (6), and the quinone is free to migrate back to the distal volume, and exit the site (7). Reduction of heme b_L changes the charge by 1, and the field changes transiently to $(1-\delta)^-$. e. The field is felt by the carboxylate of E295 (8), and the coulombic force flips it back to its initial position. f. If heme b_H is oxidized, the electron is transferred (9), and the field associated with heme b_L returns to its initial δ^+ charge. The site is now vacant, and available to accept a QH_2 for the next turnover. If heme b_L remains reduced (after the second turnover), the $(1-\delta)^-$ field serves to repel the $Q^{\bullet-}$ formed after the next cycle (reactions (1)–(3) representing a partial third turnover).

(ii) The pK $\sim$8.5 might also determine the dissociation constant for QH• in wildtype. If so, the glutamate acceptor group might be expected to have a pK similar to this or higher. In cytochrome aa_3, the glutamate at the terminus of the D-channel (water chain on the N-side of the protein) is thought to have a functional pK of $\sim$9.2 [106,107]. Since E295 in the bc_1 complex occupies a similar environment, the scenario in cytochrome aa_3 provides an example that might apply to the pK here.

Similar considerations apply to proton exit. Since water chains conduct protons freely, they must approach electrochemical equilibrium with the aqueous phase to which they are connected. At equilibrium, the activity felt within the protein at the P-side terminus must be that of the aqueous P-phase, but in flux, a difference in electrochemical potential along the chain would be present, though likely minimal. In either case, Mitchell's proton-well effect [108] would be in play, and the distribution of H^+ along the path would be determine through fractional contribution of $\Delta\psi$ to the local profile. The proton exit path is better characterized in cyt aa_3; both there and in bc_1 complex, the proton has eventually to be passed to the P-phase at pH $\leq$7.0, necessitating delivery from a group with an effective pK lower than this. The pathway in both cases involves a water chain that is also in equilibrium with a heme propionate, which might represent the terminus. It seems possible that coordination of proton and electron transfer, and the redox-linked changes in pK of the heme propionates (cf. [56,109–112]) would be

important in gating both processes. Clearly, mutagenesis of residues along the path from the Q_o-site to the aqueous phase, in association with a detailed QM/MD simulation of the changes in electrostatic profile during catalysis, will be instructive, and such studies are in progress (Wilson, C., Harrison, C., Schulten, K. and Crofts, A.R., unpublished).

It is likely that the empirical rate constants would pertain to processes that are gated [44], but details of mechanisms remain to be determined. For the high potential chain, several labs have discussed possible gating mechanisms in terms of conformations of the protein that change with changes in occupancy of the different domains of the Q_o-site [104,113,114], nicely reviewed by Berry and Huang [115]. In particular, access to the Q_o-site occupant from the P-phase (for either O_2 or ISP) is likely modulated by closure of the access port through which ISP contacts occupants. Tyr-302 is the putative "trap-door" for closure of the Q_o-site access port [104], and is also involved in stabilization of the extrinsic domain of ISP at the Q_o-site through H-bonding to the backbone $=O$ of Cys-151 of ISP. Mutation of this residue slows rates for the normal forward reaction [104,116,117], and can dramatically increase rates for SO generation [114,118], so likely this is an important player.

For the low potential chain, the choice of gating mechanism depends on choice of starting point. If a single rate constant for electron transfer pertains, the choices are limited. Osyczka et al. [44], having discounted any role for E295, suggested control by coulombic effects on dipolar orientation of waters to gate H^+ pathways. With the necessity for SQ

movement, and the essential roles for E295 envisaged here, the scope is greatly enlarged, with the most obvious mechanisms those proposed, — coulombic forces would keep $Q^{\bullet-}$ in the distal domain if heme b_L^- had a net negative charge, so that only the slow rate constants would be in effect. Similar forces would also modulate displacements of the carboxylate form of E295. In any case, reversal of the reaction would require coordination of electron and proton transfer, with many possibilities for gating, as discussed above.

4.9. A kinetic model for the Q_o-site reaction

From the considerations above, a strong case can be made for a mechanism that depends on movement of SQ in the Q_o-site to facilitate the second electron transfer. Covian et al. [31] had suggested that such a model was untenable. Their main criticism was that in the previous work [9] we had failed to take account of plausible values for diffusion coefficient of SQ in the Q_o-site. We agree that the diffusional rate constant was not properly considered in that study, but we disagree with the more general conclusion they reached, that all models involving the movement of SQ in the site are therefore untenable. In our previous discussions, we had assumed that occupancy of the SQ would be maintained as low as possible so as to minimize the probability of bypass reactions, and used Moser–Dutton values for k_2^{cat} of 4×10^6 s^{-1} from the distal domain and 4×10^9 s^{-1} from the proximal domain as primary constraints. If the movement of SQ_d to SQ_p was sufficiently rapid, the intrinsic rate would be determined by electron transfer from the proximal domain, allowing a very low occupancy. The implicit ad hoc assumption, that the rate constant for diffusion was faster than k_2^{cat} from the proximal domain, was not realistic. The original model could be readily extended to demonstrate that reduction of heme b via diffusion of SQ in the site was realistic, but it had omitted a proper representation of other essential features, in particular the competition between the forward and reverse reactions [31]. The model shown here is expanded to include all redox centers of the complex, and established partial processes [8,9]. The main considerations are SQ occupancy, now determined, and the three pairs of forward and reverse rate constants, — for electron transfer from the distal and proximal domains, and for the diffusional step. For the first electron transfer, partial processes included are formation of ES-complex, the probability for the H^+ to be in the configuration needed for electron transfer (the Brønsted barrier for formation of the active state), and the electron transfer step. Values for forward rate constants are taken from the literature or derived from well-established parameters (see Notes to Table 1), and reverse rate constants were adjusted so as to provide values for the overall equilibrium constant consistent with existing data. The value of $k_{2d} \sim 10^3$ s^{-1} for oxidation of SQ from the distal domain is that derived above from the SQ occupancy and measured rates. We have assumed that this value for rate constant would also be appropriate if $Q^{\bullet-}$ was constrained to the distal domain in wildtype. In this case, the observed rate could be explained only by some additional process increasing the rate constant, simulated here by movement of SQ closer to heme b_L. The diffusional step for SQ has been explicitly modeled. The value for diffusional rate constant, $10^7 < k_{diff} \leq 10^8$ s^{-1}, was derived from $x^2 = 2Dt$, a 1-D diffusion distance of 5.0 Å, and the diffusion coefficient for ubiquinone-10 [119] or plastoquinone [120] in the membrane. Values measured for D have been in the range 10^{-7} to 10^{-9} cm^{2}s^{-1}, depending on protein crowding, and are similar to the value for the diffusion coefficient of phospholipids in membranes ($\sim 10^{-8}$ cm^{2}s^{-1}). Since diffusion of $Q^{\bullet-}$ would involve an open volume close to heme b_L, a value at the high end of the plausible range might be appropriate. In the simulation, SQ occupancy at levels comparable to those observed experimentally requires oxidation of ISPH and ferroheme c_1 by an external acceptor to pull the reaction over beyond the first turnover (see discussion of equilibria in Section 4.2). The occupancy found depends on the equilibrium constant for this reaction, and hence the E_m of the acceptor. The value used in the model, giving $K \sim 100$, is appropriate for the

complex *in situ* (with RC or cyt oxidase as acceptor). However, as might be expected, this leads to occupancy when the oxidation of SQ is limited (for example by eliminating the diffusional step) that is, at least transiently, higher (>0.2 SQ/site) than that measured using the isolated complex and horse heart cyt c as acceptor. It should also be noted that, because of the competition from back-reaction, the range of values for k_{diff} is more severely constrained than when the model of [31] was extended (see SI).

Reactions, rate constants and values for all parameters used are shown in Table 1, and Dynafit scripts are provided in the supplementary materials. Three kinetic models are simulated using the same set of parameters: (i) a single turnover of the Q_o-site following addition of QH_2 to the oxidized complex inhibited by antimycin, allowing exploration of occupancy of SQ, and the dependence of the rate of heme b_H reduction on the diffusional step; (ii) as (i), but with equilibria for additional turnovers to allow the oxidized complex to come to equilibrium with the Q-pool; and (iii) as (ii) but with steps to allow the high potential chain to equilibrate with an acceptor pool. We note that, although all equilibrium constants used are natural, the rate constants for one process, the oxidation of cyt c_1 by added acceptor (k_3 and k_{-3}) are higher than justified by observed rates, and therefore unnatural. Lowering these values led to slowed kinetics, especially for the second turnover; we tentatively ascribe this discrepancy to gating in the high potential chain that is not included in the current model. The scripts for these models, and an early preliminary model based on [31], are available in the supplementary materials.

4.9.1. Simulation outcome

As shown in Fig. 9A, the kinetics modeled depended strongly on the value chosen for the diffusional rate constant. Rates of heme b_H reduction associated with oxidation of the first QH_2 reflected the limiting first electron transfer as long as k_{diff} was in the range $>10^7$ s^{-1}, — well within plausible estimates. Kinetics of ISP and cyt c_1 reduction summed to follow the kinetics of heme b_H reduction in the first turnover, but individual amplitudes (and initial rates) reflected the equilibrium constant between ISP and heme c_1. Note that whenever acceptors were available in both chains, the SQ occupancies (for example, with $k_{diff} = 10^7$ s^{-1}, $[SQ_d]$ was transiently $\sim 1.5 \cdot 10^{-4}$) were below the detection limits currently accessible using EPR (Fig. 9C). The model therefore accounts for the data of Zhu et al. [38], but in the context of our model. The SQ_p occupancy ($\sim 2.5 \cdot 10^{-7}$) was in the range of the minimal value we assumed in previous discussions [9,10]. When the simulation was allowed to continue into a second turnover, a slow reduction of heme b_L occurred, driven by the large excess of QH_2, but little additional SQ ($\sim 2 \cdot 10^{-5}$) accumulated (Fig. 9B, C). As seen experimentally, reduction of heme b_L developed only as reduction of heme b_H reached completion, and was slow unless additional acceptor was present. Only when an excess of acceptor for the high potential chain was included did the rates for heme b_L reduction approach experimental rates; SQ occupancy lagged heme b_L reduction, and approach the experimental range only with the heme substantially reduced (Fig. 9D). If diffusion of SQ was impeded, a high transient level of SQ was detected during the first turnover, but if SQ was able to move rapidly, significant levels developed only during the second turnover.

The changes in kinetics of SQ occupancy on changing the values of k_{diff} would model those expected between the wildtype and the E295W mutant. In the experimental context, the conditions are the same, but the mechanism by which SQ removal is inhibited is different. However, in each case, after inhibition has set in, the SQ has to reach equilibrium poise consistent with that of other reactants in the reaction. In the case of the antimycin-inhibited wildtype, two quinol equivalents are consumed (in reduction of the two b-hemes) before the inhibition leading to substantial accumulation of SQ sets in; after this delay the SQ would approach equilibrium with other components of the overall reaction. In the mutant, the removal of the SQ is inhibited from the outset, so that the SQ accumulates rapidly on oxidation of the first quinol

Table 1

Partial processes and kinetic parameters for Q_o-site model.

Reaction equation	Rate constants		$k_{forward}$	$k_{reverse}$	K_{eq}	
$EFeS.c_1.b_L.b_H + QH_2 \rightleftharpoons EFeS.c_1.b_L.b_H.QH_2$	k_{onQH}	k_{off}	$500 \times [QH_2]$	5×10^3	10	a
$EFeS.c_1.b_L.b_H.QH_2 \rightleftharpoons EFeS.c_1.b_L.b_H.QH\text{-}H$	k_{proton}	$k_{-proton}$	10^7	10^{12}	10^{-5}	b
$EFeS.c_1.b_L.b_H.QH\text{-}H \rightleftharpoons EFeS^-.c_1.b_L.b_H.SQ(d)$	k_1	k_{-1}	1.65×10^8	3.25×10^5	510	c
$EFeS^-.c_1.b_L.b_H.SQ(d) \rightleftharpoons EFeS.c_1^-.b_L.b_H.SQ(d)$	k_5	k_{-5}	10^8	3×10^8	0.33	d
$EFeS.c_1^-.b_L.b_H.SQ(d) + A_{ox} \rightleftharpoons EFeS.c_1.b_L.b_H.SQ(d) + A_{red}$	k_3	k_{-3}	10^7	10^5	100	e
$EFeS.c_1.b_L.b_H.SQ(d) \rightleftharpoons EFeS.c_1.b_L^-.b_H.Q(d)$	k_{2d}	k_{-2d}	1.2×10^3	0.192	6250	f
$EFeS.c_1.b_L^-.b_H.Q(d) \rightleftharpoons EFeS.c_1.b_L.b_H^-.Q(d)$	k_4	k_{-4}	10^6	6250	160	g
$EFeS.c_1.b_L.b_H.SQ(d) \rightleftharpoons EFeS.c_1.b_L.b_H.SQ(p)$	k_{diff}	k_{-diff}	10^7	10^7	1	h
$EFeS.c_1.b_L^-.b_H^-.SQ(d) \rightleftharpoons EFeS.c_1.b_L^-.b_H^-.SQ(p)$	k_{diff3}	k_{-diff3}	10^6	10^8	0.01	h
$EFeS.c_1.b_L.b_H.SQ(p) \rightleftharpoons EFeS.c_1.b_L^-.b_H.Q(p)$	k_{2p}	k_{-2p}	4.3×10^9	6.9×10^5	6250	i
$EFeS.c_1.b_L^-.b_H.Q(p) \rightleftharpoons EFeS.c_1.b_L.b_H^-.Q(p)$	k_4	k_{-4}	10^6	6250	160	g
$EFeS.c_1.b_L.b_H^-.Q(p) \rightleftharpoons EFeS.c_1.b_L.b_H^-.Q(d)$	k_{diff}	k_{diff}	10^7	10^7	1	h
$EFeS.c_1.b_L.b_H^-.Q(d) \rightleftharpoons EFeS.c_1.b_L.b_H^- + Q$	k_{off}	k_{onQ}	5×10^3	$50 \times [Q]$	1	j
$EFeS.c_1.b_L.b_H^- + QH_2 \rightleftharpoons EFeS.c_1.b_L.b_H^-.QH_2$	k_{off}	k_{onQH}	$500 \times [QH_2]$	5×10^3	10	k

Notes:

The model represents the essential processes of the Q_o-site reaction, constrained by antimycin to prevent the Q_i-site reaction so that flux out of the b-heme chain is inhibited. The full complement of redox centers is included, and an additional acceptor (by default in 6-fold excess over the complex) of $E_{m,7}$ 420 mV to simulate the driving force available from the rest of the chain. For simplicity, it is assumed that all components retain the $E_{m,7}$ values determined by redox titration. The reactions shown are appropriate to the first turnover of the Q_o-site. The model allows simulation of the second turnover, and uses the same rate constants for similar processes (see Supplementary Information for details).

a) The value for k_{onQH} shown is that suggested in [31], with the initial $[QH_2]$ given as 200 (no units), to give an apparent first-order rate constant of 5×10^4 s^{-1}. In chromatophores at saturating QH_2, the exchange of Q and QH_2 has no appreciable contribution to the kinetics [72], indicating that these reactions are all rapid compared to the rate limiting step. The second-order rate constant determined in situ was $\sim 2 \times 10^5$ M^{-1} s^{-1} [74], estimated from the observed rate at $\sim$10 mM QH_2 in the membrane. The diffusion-limited rate constant would be considerably higher. The displacement of the apparent E_m due to formation of the ES_1-complex shows a tighter binding of QH_2 than Q by a factor $\sim$10.

b) Rates for H$^+$ exchange along H-bonds have been variously estimated on the range 10^{11} to 10^{13} s^{-1} [123–125]. We have used a value of 10^{12} s^{-1} for $k_{-proton}$, the more rapid of the two rate constants, but any choice in the range shown experimentally would give the same kinetics overall. The ratio of rate constants gives the probability for finding the H$^+$ in a position favorable for electron transfer (the equilibrium constant for distribution along the H-bond), derived from the difference in pK values between donor (the –OH of QH_2, p$K > 11.5$) and acceptor groups (the N$_\varepsilon$ of His-152 (His-161 in mitochondrial sequences) of the oxidized ISP, with p$K_{ox1} \sim 7.6$). At saturating QH_2, electron transfer occurs from the ES_1-complex, and the value for pK_{ox1} would be less than in the isolated ISP because of the binding free-energy [8]. A value of 6.5 is used in the simulation (a ΔpK of 10^5).

c) The forward rate constant is that for electron transfer from the weakly populated configuration in which the H$^+$ is close to the histidine N$_\varepsilon$ of His-152 (occupancy 10^{-5} used here, see (b)). The value for rate constant needed to match the observed rate is therefore 10^5-fold greater than the observed value. The value given here is that from a Marcus analysis using the distance dependence of Moser and colleagues [100], and $\lambda = 0.935$, distance 7.0 Å, and driving force $\Delta G^o/F = -0.16$ V appropriate to the value for K_{eq} shown. The reverse rate constant is chosen to give a SQ occupancy in the range shown by experiment ($\sim$0.05 [30] and this work), after taking account of the occupancy of the intermediate state. It is assumed that the reaction is reversible only in the ES_1-complex configuration. After electron transfer, the H-bond to SQ would break, releasing the reduced ISP, which would rapidly rotate away from the ES-complex configuration to passes its electron to heme c_1.

d) Removal of ISPH from interaction with Q_o-site, and oxidation to ISP$_{ox}$. The forward rate constant given is that for dissociation and movement of ISPH, since this would release SQ for further reaction. The equilibrium constant is that for oxidation of ISPH by cyt c_1, which is weakly unfavorable at pH 7.0.

e) Second-order rate constant to represent oxidation of cyt c_1 by a pool of high-potential acceptor.

f) The forward rate constant for oxidation of SQ in the domain distal from heme b_L. The value is that needed to match the observed rate in strains mutated at Glu-295 ($v \sim$40–80 QH_2/bc_1/s at pH 8.5–9), with a SQ occupancy $\sim$0.05 [30], using the relation, $v = k$(occupancy).

g) The rate constant for electron transfer from heme b_L to heme b_H. The forward rate constant was calculated using Marcus/Moser–Dutton analysis from the distance given by modeling. The reverse rate constant was chosen so that the equilibrium constant matches that calculated from E_m values. The value is similar to that determined from the rate of oxidation of heme b_H induced by generation of a membrane potential [126]. The kinetics of heme b_H reduction were not significantly changed by varying the value for k_4 over the range 10^4 to 10^6 s^{-1}, though a transient reduction of heme b_L (maximal occupancy 0.08) was seen when the lower value was used.

h) An approximate value for k_{diff} is given by $k \approx 1/t = 2D / <x^2>$. Using $x = 5 \times 10^{-8}$ cm, D in the range 10^{-9} to 10^{-7} cm^2 s^{-1} [119,120], we find $0.8 \times 10^6 < k_{diff} < 0.8 \times 10^8$ s^{-1}, assuming a 1-dimensional diffusion path, and diffusion in both directions from a starting position; if movement was constrained to the direction closer to heme b_L, the values would scale up. The value used in the simulation could be varied over the range 10^8–10^7 s^{-1} without changing the overall rate of reaction. In all the simulations shown in which heme b_L was available in the oxidized form, the same value was used in forward and reverse directions. The limited range could be extended by applying a bias to the diffusional process. For example, bias would increase k_{diff} if there was a coulombic driving force for displacement of Q$^{\bullet-}$ by a positive field around heme b_L. Similarly, the occupancy of the distal domain by Q$^{\bullet-}$ could be constrained if k_{-diff} was increased by a negative field around ferroheme b_L. In the simulation, we implemented such an effect under conditions in which both b-hemes were reduced, but the only outcome affected was the distribution between SQ_d and SQ_p states. In the mechanism outlined in Fig. 8 we speculate that the change in charge on reduction would switch the field from +ve to −ve, but have not otherwise implemented that feature in the present models. For the neutral Q species, the same value for k_{diff} was used in both reaction directions. The value for k_{diff} was varied in the plots of Figs. 7–9, as indicated, to simulate impaired oxidation of SQ by mutation of Glu-295.

i) The forward rate constant for oxidation of SQ in the domain proximal to heme b_L. The value was calculated using the Moser–Dutton distance parameter, the distance to heme b_L shown by myxothiazol-containing structures, and the Marcus exponential term [8]. Both here, and in estimation of the complementary parameter for the distal domain, the reverse rate constant was calculated so as to be consistent with the equilibrium for the overall reaction and the other values for equilibrium constants used in the simulation.

j) The values chosen reflect a 10-fold tighter binding for QH_2 than Q at the catalytic site. As noted in a), the actual value is conservative.

k) Because of the 25 Å distance, and the neutral charged state of the binding species, it was assumed that the redox state of heme b_H did not affect the binding of Q or QH_2 at the Q_o-site.

(on activation via oxidation of the high-potential chain in chromatophores), in transient equilibrium with the reactants of the first electron transfer, but the poise of the second electron transfer reaches equilibrium on a much slower time scale, due to the inhibited delivery of electrons to heme b_L. These effects can be seen in the kinetics modeled in Fig. 9F. The consequence of the different time courses is that the occupancy of SQ in the two strains at any particular time will be different, but will approach the same value at longer times. The occupancy in the wildtype approaches equilibrium from below, and that in E295W from above, so that occupancy in the former would be lower than in

the latter at any time prior to that at which both had reached equilibrium, consistent with the difference observed experimentally.

When a large pool of acceptor was provided, and an additional reaction step for oxidation of the SQ by O_2 was included, the steady-state flux of SO generation could also be modeled, with rate dependent on choice of rate constant (not shown).

The kinetic limitation in the E295 mutants could in principle come from any partial process in the second electron transfer, including the pathway for proton exit, but was modeled here simply by decreasing the rate constant for the diffusional state. Software constraints limit
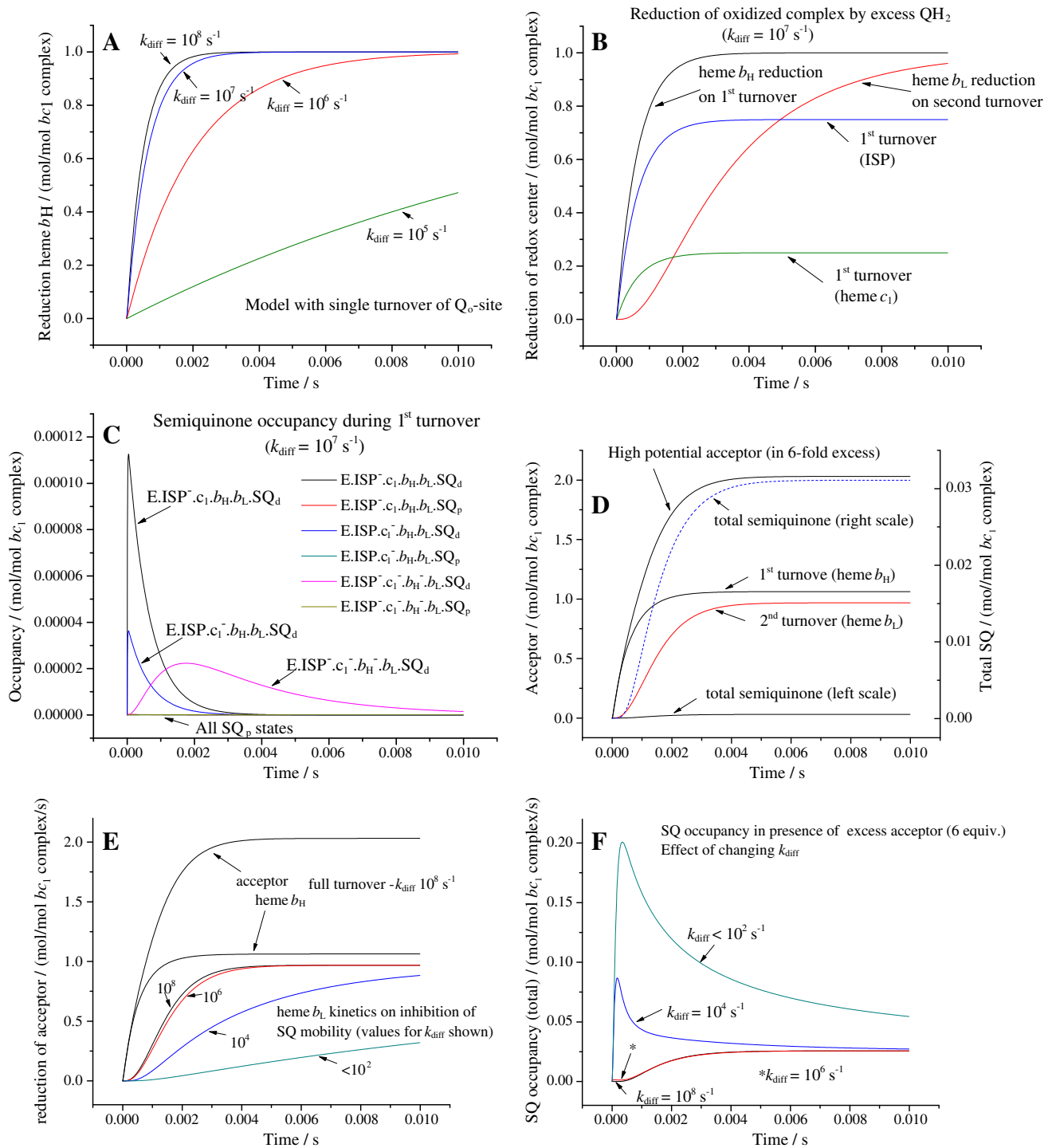
Fig. 9. Simulated kinetic curves on addition of QH_2 to the oxidized bc_1 complex. A. Kinetics in the first turnover to show the effect on turnover of slowing the diffusion of SQ from distal to proximal domains of the Q_o-site by changing k_{diff}. B. Kinetics on reduction by adding 200-fold excess of QH_2 to the oxidized complex in the absence of additional acceptor. The reduction of heme b_L reflects a second turnover driven by the excess QH_2. C. Occupancy of different states in which the SQ was significantly populated during the first turnover. D. Kinetics in the presence of 6-fold excess of acceptor for the high-potential chain. Heme b_L becomes reduced only after heme b_H, and high occupancy of SQ lags reduction of heme b_L. The right-hand scale is appropriate for the dashed trace, amplified to show SQ kinetics. E. Kinetics to show the dependence of heme b_L reduction (second turnover) on SQ mobility. F. Kinetics of SQ occupancy with different degrees of inhibition of SQ diffusion. As diffusion becomes severely limited, the SQ occupancy builds up during the first turnover, and then relaxes to the equilibrium value as electrons pass through to the b-heme chain. Note that, apart from a slight increase in occupancy during the first two turnovers (*), the SQ accumulating during the third partial turnover has the same kinetics over the range of values for k_{diff} between 10^8 and 10^6 s^{-1} (c.f. frame D).

the complexity of the kinetic model, and, apart from provisions for testing coulombic bias, we did not attempt to extend it to include separate partial processes for gating mechanisms, or for the proton exit pathway via E295, which we assume to be rapid in wildtype compared to the rate limiting step.

4.9.2. Inhibition by antimycin

Ransac et al. [102,121], had pointed out that their stochastic kinetic models allowed the equilibrations that open up the bypass processes discussed by Osyzcka et al. [44], and that as a consequence, inhibition by antimycin could not be modeled without ad hoc additions to the

model. Instead, the bifurcated reaction was essentially decoupled, as also emphasized by Moser et al. [122]. In their choice of rate constants, each of these groups had assumed that the second electron transfer involved a single rate constant for SQ oxidation calculated from distance, with SQ constrained to the location of its generation, — the distal domain in [102], some intermediate location in [44]. Kim et al. [101] in an exercise using similar constraints reached a similar conclusion. It might be expected from this that in the more severely crippled E295 mutant strains, a marked decoupling would also be observed. However, the bypass rates in these strains were in the same range as in antimycin inhibited wildtype, which showed almost complete inhibition. As noted above, with a known SQ occupancy under conditions in which bypass reactions occur at a measured rate, empirical values for rate constants of particular bypass processes (reduction of SQ by heme b_L^-, reduction of O_2 or ISP_{ox} by SQ) can be calculated, and applied in modeling rates for the states in which SQ accumulates. In the present model, we have not included these processes because we do not know what additional partial processes are involved, but the empirical rate constants discussed would lead to the strongly inhibited rates observed. By introducing the diffusional step in the second electron transfer, we open the possibility of the gating envisaged in [44]. Control of the bifurcated reaction to minimize reduction of SQ by heme b_L^- might involve a restriction of SQ to the distal domain by the coulombic mechanism previously proposed, and we have included such as a token. However, in the absence of these additional processes, it has no effect. The model simulates the essential features of the forward Q_o-site reaction, and provides a starting point for a more complete study in which further complexities associated with control and gating of the reaction *in situ* can be explored.

5. Conclusions

1) From the work establishing the role of ISP_{ox} [27,62,81], and from the changes in pH dependence compared to wildtype in ISP and E295 mutants, it is clear that the changed profile in the latter is not a direct consequence of loss of the glutamate sidechain, but reflects a change in the rate limiting process from the first to the second electron transfer. The pK at ~8.5 is due to dissociation of some other group to a form that favors electron transfer. A plausible candidate is the dissociation of the neutral SQ to the anionic form: $QH^{\bullet} \rightleftharpoons Q^{\bullet-} + H^+$.

2) Contrary to previous conclusions [55,56], mutation of E295 severely lowers the rate constant for oxidation of SQ by heme b_L. However, the data do not allow an unambiguous distinction between roles in the electron and proton transfer. The pattern of Zn-inhibition is consistent with a role in proton exit [52]. Our original hypothesis [24] was driven by the rotational displacement of the sidechain needed to fulfill this role, clearly demonstrated by the changes in E295 configuration seen in structures with stigmatellin [19,26] compared to those with myxothiazol (or other MOA-inhibitors) [26,50]. The structures also showed occupancy of the volume proximal to heme b_L by the MOA-class of inhibitors [26,50]. As noted before [26], the effects seen when residues impinging on this volume are mutated, the differential sensitivity to the two classes of inhibitor, the slowing of electron transfer observed in these mutants, and the lack of effect on binding in the distal domain, strongly hint at a need for occupancy of the proximal domain by an intermediate state. In the absence of inhibitor, rotational displacement of the E295 sidechain would open the volume to SQ if the latter were mobile. The properties revealed by interactions with local nuclear magnets [30] are consistent with such mobility, and our kinetic modeling demonstrates that, with these factors incorporated, movement of SQ in the site is plausible, and is sufficient to account for the high rates observed in the wildtype. In the hypothesis tested, both the direct role in H^+ exit, and the indirect role in facilitating electron transfer would be necessary, but choice of which is the step inhibited depends on the

dissociation sate of SQ. If $Q^{\bullet-}$ is the form of SQ accumulated in the E295 mutants, then dissociation is not rate limiting, and inhibited movement in the site is the best explanation. We believe that in E295W the case is strong, but recognize that the balance could flip in the other direction in other mutants, and our current studies are aimed at resolving this uncertainty.

3) The occupancy measured here in E295W under conditions of favorable driving force, together with the constraint on mobility from the bulk of tryptophan, provides a plausible basis for calculation of a rate constant for oxidation of SQ from the distal domain. The value obtained is >1000-fold lower than that calculated for electron transfer over the distance from the distal domain to heme b_L. Starting there, two explanations for the inhibition observed in E295 mutants seem plausible. i) If the SQ species detected in E295W is $Q^{\bullet-}$, the inhibition must be in some step after dissociation, likely movement of SQ. In that case, the rate constant calculated would be appropriate in the native complex and would exclude explanations for the rapid rates seen in uninhibited systems based on electron transfer from $Q^{\bullet-}$ that remains in the distal domain. We believe the weight of evidence supports this explanation. ii) If the SQ species is QH•, then dissociation could well be the inhibited step, the rate constant measured would pertain to that form, and a different value might pertain in the wildtype mechanism. As noted in the previous paragraph, the hypothesis is framed in the context of a straightforward test.

4) With the qualifications above, we can claim that the main features of the hypothesis sketched out a dozen years ago [24] are now supported by experimental data. The results are consistent with a plausible mechanism for this second step of the bifurcated reaction, and suggest a molecular ballet, with E295 as the prima ballerina, whose choreography is directed by coulombic interactions that implement control functions. In the mechanism we propose, and in contrast to previous proposals [56], the participation of E295 lowers energy barriers for the forward reaction as in the conventional view of catalysis, but raises them towards the bypass reactions by exploiting separate pathways for electron and proton, the spatial separation between the distal domain (at which SQ is generated) and the proximal domain (close enough to acceptor heme b_L for rapid oxidation), the mobility of the SQ, and the potential for gating in the flexibility of conformation in the Q_o-site, and a dance, frozen in the structures, whose step-by-step choreography remains to be explored.

Acknowledgements

Appendix A. Supplementary data

Supplementary data to this article can be found online at http://dx.doi.org/10.1016/j.bbabio.2012.10.012.

References

[1] E.A. Berry, D.-W. Lee, L.-S. Huang, F. Daldal, Structural and mutational studies of the cytochrome bc_1 Complex, in: C.N. Hunter, F. Daldal, M.C. Thurnauer, J.T. Beatty (Eds.), The Purple Phototrophic Bacteria, Springer, Dordrecht, The Netherlands, 2009.

[2] A.R. Crofts, The cytochrome bc_1 complex — function in the context of structure, Annu. Rev. Physiol. (2004) 689–733.

[3] A.R. Crofts, S.W. Meinhardt, K.R. Jones, M. Snozzi, The role of the quinone pool in the cyclic electron-transfer chain of *Rhodopseudomonas sphaeroides*: a modified Q-cycle mechanism, Biochim. Biophys. Acta 723 (1983) 202–218.

[4] P. Mitchell, Proton motive redox mechanism of the cytochrome b-c₁ complex in the respiratory chain: proton motive ubiquinone cycle, FEBS Lett. 56 (1975) 1–6.

[5] P. Mitchell, Possible molecular mechanisms of the protonmotive function of cytochrome systems, J. Theor. Biol. 62 (1976) 327–367.

[6] A.R. Crofts, The Q-cycle, — a personal perspective, Photosynth. Res. 80 (2004) 223–243.

[7] S.J. Hong, N. Ugulava, M. Guergova-Kuras, A.R. Crofts, The energy landscape for ubihydroquinone oxidation at the Q_o-site of the bc_1 complex in *Rhodobacter sphaeroides*, J. Biol. Chem. 274 (1999) 33931–33944.

[8] A.R. Crofts, Proton-coupled electron transfer at the Q_o-site of the bc_1 complex controls the rate of ubihydroquinone oxidation, Biochim. Biophys. Acta 1655 (2004) 77–92.

[9] A.R. Crofts, S. Lhee, S.B. Crofts, J. Cheng, S. Rose, Proton pumping in the bc_1 complex: a new gating mechanism that prevents short circuits, Biochim. Biophys. Acta 1757 (2006) 1019–1034.

[10] A.R. Crofts, J.T. Holland, D. Victoria, D.R. Kolling, S.A. Dikanov, R. Gilbreth, S. Lhee, R. Kuras, M.G. Kuras, The Q-cycle reviewed: how well does a monomeric mechanism of the bc_1 complex account for the function of a dimeric complex? Biochim. Biophys. Acta 1777 (2008) 1001–1019.

[11] E. Denke, T. Merbitz-Zahradnik, O.M. Hatzfeld, C.H. Snyder, T.A. Link, B.L. Trumpower, Alteration of the midpoint potential and catalytic activity of the iron–sulfur protein by changes of amino acids forming hydrogen bonds to the iron–sulfur cluster, J. Biol. Chem. 273 (1998) 9085–9093.

[12] T. Schröter, O.M. Hatzfeld, S. Gemeinhardt, M. Korn, T. Friedrich, B. Ludwig, T. Link, Mutational analysis of residues forming hydrogen bonds in the Rieske [2Fe2S] cluster of the cytochrome bc_1 complex of *Paracoccus denitrificans*, Eur. J. Biochem. 255 (1998) 100–106.

[13] S. Lhee, D.R. Kolling, S.K. Nair, S.A. Dikanov, A.R. Crofts, Modifications of protein environment of the [2Fe-2S] cluster of the bc_1 complex: effects on the biophysical properties of the Rieske iron–sulfur protein and on the kinetics of the complex, J. Biol. Chem. 285 (2009) 9233–9248.

[14] H. Rottenberg, R. Covian, B.L. Trumpower, Membrane potential greatly enhances superoxide generation by the cytochrome bc_1 complex reconstituted into phospholipid vesicles, J. Biol. Chem. 284 (2009) 19203–19210.

[15] B.N. Ames, M.K. Shigenaga, T.M. Hagen, Oxidants, antioxidants, and the degenerative diseases of aging, Proc. Natl. Acad. Sci. U. S. A. 90 (1993) 7915–7921.

[16] D. Harman, Free radical theory of aging, in: I. Emerit, B. Chance (Eds.), Free Radicals and Aging, Birkhauser Verlag, Basel., 1992

[17] F.L. Muller, M.S. Lustgarten, Y. Jang, A. Richardson, H.V. Remmen, Trends in oxidative aging theories, Free Radic. Biol. Med. 43 (2007) 477–503.

[18] D. Xia, C.-A. Yu, H. Kim, J.-Z. Xia, A.M. Kachurin, L. Zhang, L. Yu, J. Deisenhofer, Crystal structure of the sytochrome bc_1 somplex from bovine heart mitochondria, Science 277 (1997) 60–66.

[19] Z. Zhang, L.-S. Huang, V.M. Shulmeister, Y.-I. Chi, K.-K. Kim, L.-W. Hung, A.R. Crofts, E.A. Berry, S.-H. Kim, Electron transfer by domain movement in cytochrome bc_1, Nature (Lond.) 392 (1998) 677–684.

[20] S. Iwata, J.W. Lee, K. Okada, J.K. Lee, M. Iwata, B. Rasmussen, T.A. Link, S. Ramaswamy, B.K. Jap, Complete structure of the 11-subunit bovine mitochondrial cytochrome bc_1 complex, Science 281 (1998) 64–71.

[21] C. Hunte, J. Koepke, C. Lange, T. Roßmanith, H. Michel, Structure at 2.3 Å resolution of the cytochrome bc_1 complex from the yeast *Saccharomyces cerevisiae* co-crystallized with an antibody F_v fragment, Structure 8 (2000) 669–684.

[22] E.A. Berry, L.-S. Huang, L.K. Saechao, N.G. Pon, M. Valkova-Valchanova, F. Daldal, X-ray structure of *Rhodobacter capsulatus* cytochrome bc_1: comparison with its mitochondrial and chloroplast counterparts, Photosynth. Res. 81 (2004) 251–275.

[23] L. Esser, M. Elberry, F. Zhou, C.-A. Yu, L. Yu, D. Xia, Inhibitor complexed structures of the cytochrome bc_1 complex from the photosynthetic bacterium *Rhodobacter sphaeroides*, J. Biol. Chem. 283 (2008) 2846–2857.

[24] A.R. Crofts, S.J. Hong, N. Ugulava, B. Barquera, R. Gennis, M. Guergova-Kuras, E.A. Berry, Pathways for proton release during ubihydroquinone oxidation by the bc_1 complex, Proc. Natl. Acad. Sci. U. S. A. 96 (1999) 10021–10026.

[25] E.A. Berry, L.S. Huang, Observations concerning the quinol oxidation site of the cytochrome bc_1 complex, FEBS Lett. 555 (2003) 13–20.

[26] A.R. Crofts, B. Barquera, R.B. Gennis, R. Kuras, M. Guergova-Kuras, E.A. Berry, Mechanism of ubiquinol oxidation by the bc_1 complex: the different domains of the quinol binding pocket, and their role in mechanism, and the binding of inhibitors, Biochemistry 38 (1999) 15807–15826.

[27] M. Guergova-Kuras, R. Kuras, N. Ugulava, I. Hadad, A.R. Crofts, Specific mutagenesis of the Rieske iron sulfur protein in *Rhodobacter sphaeroides* shows that both thermodynamic gradient and the pK of the oxidized form determine the rate of quinol oxidation by the bc_1 complex, Biochemistry 39 (2000) 7436–7444.

[28] K.-L. Hsueh, W.M. Westler, J.L. Markley, NMR investigations of the Rieske protein from *Thermus thermophilus* support a coupled proton and electron transfer mechanism, J. Am. Chem. Soc. 132 (2010) 7908–7918.

[29] Y. Zu, M.M.-J. Couture, D.R.J. Kolling, A.R. Crofts, L.D. Eltis, J.A. Fee, J. Hirst, The reduction potentials of Rieske clusters: the importance of the coupling between oxidation state and histidine protonation state, Biochemistry 42 (2003) 12400–12408.

[30] J.L. Cape, M.K. Bowman, D.M. Kramer, A semiquinone intermediate generated at the Q_o site of the cytochrome bc_1 complex: Importance for the Q-cycle and superoxide production, Proc. Natl. Acad. Sci. U. S. A. 104 (2007) 7887–7892.

[31] R. Covián, B.L. Trumpower, The rate-limiting step in the cytochrome bc_1 complex is not changed by inhibition of cytochrome b-dependent deprotonation: implications for the mechanism of ubiquinol oxidation at center P of the bc_1 complex, J. Biol. Chem. 284 (2009) 14359–14367.

[32] H. Zhang, A. Osyczka, P.L. Dutton, C.C. Moser, Exposing the complex III Q_o semiquinone radical, Biochim. Biophys. Acta 1767 (2007) 883–887.

[33] A.R. Crofts, Z. Wang, How rapid are the internal reactions of the ubiquinol:cytochrome c_2 oxidoreductase? Photosynth. Res. 22 (1989) 69–87.

[34] J.A. Roberts, J.P. Kirby, S.T. Wall, D.G. Nocera, Electron transfer within ruthenium(II) polypyridyl-(salt bridge)-dimethylaniline acceptor-donor complexes, Inorg. Chim. Acta 263 (1997) 395–405.

[35] M. Snozzi, A.R. Crofts, Electron transport in chromatophores from *Rhodopseudomonas sphaeroides* GA fused with liposomes, Biochim. Biophys. Acta 766 (1984) 451–463.

[36] A.R. Crofts, J.T. Holland, D. Victoria, D.R. Kolling, S.A. Dikanov, R. Gilbreth, S. Lhee, R. Kuras, M.G. Kuras, The Q-cycle reviewed: How well does a monomeric mechanism of the bc_1 complex account for the function of a dimeric complex? Biochim. Biophys. Acta 1777 (2008) 1001–1019.

[37] H. Zhang, S.E. Chobot, A. Osyczka, C.A. Wraight, P.L. Dutton, C.C. Moser, Quinone and non-quinone redox couples in Complex III, J. Bioenerg. Biomembr. 40 (2008) 493–499.

[38] J. Zhu, T. Egawa, S.R. Yeh, L. Yu, Y. CA, Simultaneous reduction of iron–sulfur protein and cytochrome b_L during ubiquinol oxidation in cytochrome bc_1 complex, Proc. Natl. Acad. Sci. U. S. A. 104 (2007) 4864–4869.

[39] H. Kim, D. Xia, C.A. Yu, J.Z. Xia, A.M. Kachurin, L. Zhang, L. Yu, J. Deisenhofer, Inhibitor binding changes domain mobility in the iron–sulfur protein of the mitochondrial bc1 complex from bovine heart, Proc. Natl. Acad. Sci. U. S. A. 95 (1998) 8026–8033.

[40] C. Hunte, H. Palsdottir, B.L. Trumpower, Protonmotive pathways and mechanisms in the cytochrome bc_1 complex, FEBS Lett. 545 (2003) 39–46.

[41] A. Osyczka, C.C. Moser, F. Daldal, P.L. Dutton, Reversible redox energy coupling in electron transfer chains, Nature 427 (2004) 607–612.

[42] S. Bartoschek, M. Johansson, B.H. Geierstanger, J.G. Okun, C.R.D. Lancaster, E. Humpfer, L. Yu, C.-A. Yu, C. Griesinger, U. Brandt, Three molecules of ubiquinone bind specifically to mitochondrial cytochrome bc_1 complex, J. Biol. Chem. 276 (2001) 35231–35234.

[43] H. Ding, C.C. Moser, D.E. Robertson, M.K. Tokito, F. Daldal, P.L. Dutton, Ubiquinone pair in the Qo site central to the primary energy conversion reactions of cytochrome bc_1 complex, Biochemistry 34 (1995) 15979–15996.

[44] A. Osyczka, C.C. Moser, P.L. Dutton, Fixing the Q-cycle, Trends Biochem. Sci. 30 (2005) 176–182.

[45] T.A. Link, The role of the 'Rieske' iron sulfur protein in the hydroquinone oxidation (Q(P)) site of the cytochrome bc_1 complex. The 'proton-gated affinity change' mechanism, FEBS Lett. 412 (1997) 257–264.

[46] E.A. Berry, L.S. Huang, Observations concerning the quinol oxidation site of the cytochrome bc_1 complex, FEBS Lett. 555 (2003) 13–20.

[47] A.R. Crofts, M. Guergova-Kuras, L.-S. Huang, R. Kuras, Z. Zhang, E.A. Berry, The mechanism of ubiquinol oxidation by the bc_1 complex: the role of the iron sulfur protein, and its mobility, Biochemistry 38 (1999) 15791–15806.

[48] A.R. Crofts, M. Guergova-Kuras, N. Ugulava, R. Kuras, S. Hong, Proton processing at the Q_o-site of the bc_1 complex of *Rhodobacter sphaeroides*, in: Proc. XIIth Congress of Photosynthesis Research, Brisbane, Australia, 2002, p. 6.

[49] S. Izrailev, A.R. Crofts, E.A. Berry, K. Schulten, Steered molecular dynamics simulation of the Rieske subunit motion in the cytochrome bc_1 complex, Biophys. J. 77 (1999) 1753–1768.

[50] L. Esser, B. Quinn, Y.-F. Li, M. Zhang, M. Elberry, L. Yu, C.-A. Yu, D. Xia, Crystallographic studies of quinol oxidation site inhibitors: A modified classification of inhibitors for the cytochrome bc_1 complex, J. Mol. Biol. 341 (2004) 281–302.

[51] C. Hunte, S. Solmaz, H. Palsdóttir, T. Wenz, A structural perspective on mechanism and function of the cytochrome bc_1 complex, in: Bioenergetics, Springer, Berlin / Heidelberg, 2008, pp. 253–278.

[52] D.-W. Lee, Y. El Khoury, F. Francia, B. Zambelli, S. Ciurli, G. Venturoli, P. Hellwig, F. Daldal, Zinc inhibition of bacterial cytochrome bc_1 reveals the role of cytochrome b E295 in proton release at the Qo site, Biochemistry 50 (2011) 4263–4272.

[53] M. Castellani, R. Covian, T. Kleinschroth, O. Anderka, B. Ludwig, B.L. Trumpower, Direct demonstration of half-of-the-sites reactivity in the dimeric cytochrome bc_1 complex, J. Biol. Chem. 285 (2010) 502–510.

[54] M. Świerczek, E. Cieluch, M. Sarewicz, A. Borek, C.C. Moser, P.L. Dutton, A. Osyczka, An electronic bus bar lies in the core of cytochrome bc_1, Science 329 (2010) 451–454.

[55] T. Wenz, P. Hellwig, F. MacMillan, B. Meunier, C. Hunte, Probing the role of E272 in quinol oxidation of mitochondrial complex III, Biochemistry 45 (2006) 9042–9052.

[56] A. Osyczka, H. Zhang, C. Mathé, P.R. Rich, C.C. Moser, P.L. Dutton, Role of the PEWY glutamate in hydroquinone-quinone oxidation-reduction catalysis in the Q_o site of cytochrome bc_1, Biochemistry 45 (2006) 10492–10503.

[57] M. Guergova-Kuras, R. Salcedo-Hernandez, G. Bechmann, R. Kuras, R.B. Gennis, A.R. Crofts, Expression and one-step purification of a fully active polyhistidine-tagged cytochrome bc_1 complex from *Rhodobacter sphaeroides*, Protein Expr. Purif. 15 (1999) 370–380.

[58] R. Kuras, M. Guergova-Kuras, A.R. Crofts, Steps toward constructing a cytochrome b_6f complex in the purple bacteria *Rhodobacter sphaeroides*: An example of the structural plasticity of a membrane cytochrome, Biochemistry 37 (1998) 16280–16288.

[59] S.W. Meinhardt, A.R. Crofts, The Role of Cytochrome b_{566} in the Electron Transfer Chain of *Rps. sphaeroides*, Biochim. Biophys. Acta 723 (1983) 219–230.

[60] J.R. Bowyer, S.W. Meinhardt, G.V. Tierney, A.R. Crofts, Resolved difference spectra of redox centers involved in photosynthetic electron flow in *Rhodopseudomonas capsulata* and *Rps. sphaeroides*, Biochim. Biophys. Acta 635 (1981) 167–186.

[61] S.W. Meinhardt, A.R. Crofts, Kinetic and thermodynamic resolution of cytochrome c_1 and cytochrome c_2 from *Rps. sphaeroides*, FEBS Lett. 149 (1982) 223–227.

[62] S. Lhee, D.R. Kolling, S.K. Nair, S.A. Dikanov, A.R. Crofts, Modifications of protein environment of the [2Fe-2S] cluster of the bc_1 complex: effects on the biophysical properties of the Rieske iron–sulfur protein and on the kinetics of the complex, J. Biol. Chem. 285 (2010) 9233–9248.

[63] P. Kuzmic, Program DYNAFIT for the analysis of enzyme kinetic data: Application to HIV proteinase, Anal. Biochem. 237 (1996) 260–273.

[64] J.R. Bowyer, G.V. Tierney, A.R. Crofts, Secondary electron transfer in chromatophores of *Rhodopseudomonas capsulata* A1a pho$^-$ - binary oscillations, FEBS Lett. 101 (1979) 201–206.

[65] A.R. Crofts, C.A. Wraight, The electrochemical domain of photosynthesis, Biochim. Biophys. Acta 726 (1983) 149–186.

[66] N.G. Holmes, A.R. Crofts, The carotenoid shift in *Rhodopseudomonas sphaeroides*; the flash-induced change, Biochim. Biophys. Acta 459 (1977) 492–505.

[67] J.B. Jackson, A.R. Crofts, The high energy state in chromatophores from *Rhodopseudomonas spheroides*, FEBS Lett. 4 (1969) 185–189.

[68] A.R. Crofts, The chromatophore as a functional unit, in: J.M. Tager, S. Papa, E. Quagliariello, E.C. Slater (Eds.), Electron Transport and Energy Conservation, Adriatica Editrice, Bari, Italy, 1970, pp. 221–228.

[69] A.R. Crofts, J.B. Jackson, The high energy state in chromatophores from photosynthetic bacteria, in: J.M. Tager, S. Papa, E. Quagliariello, E.C. Slater (Eds.), Electron Transport and Energy Conservation, Adriatica Editrice, Bari, Italy, 1970, pp. 383–408.

[70] A.R. Crofts, R.J. Cogdell, J.B. Jackson, The relation of H$^+$-uptake to electron flow in photosynthetic bacteria, in: G.F. Azzone, L. Ernster, S. Papa, E. Quagliariello, N. Siliprandi (Eds.), Mechanisms in Bioenergetics, Academic Press, New York and London, 1973, pp. 337–346.

[71] A.R. Crofts, J.B. Jackson, E.H. Evans, R.J. Cogdell, The high-energy state in chloroplasts and chromatophores, in: Proc. IInd. International Cong. on Photosynthesis, Stresa, 1971, 1972.

[72] A.R. Crofts, V.P. Shinkarev, D.R.J. Kolling, S. Hong, The modified Q-cycle explains the apparent mismatch between the kinetics of reduction of cytochromes c_1 and b_H in the bc_1 complex, J. Biol. Chem. 278 (2003) 36191–36201.

[73] J.B. Jackson, A.R. Crofts, The kinetics of light induced carotenoid changes in *Rhodopseudomonas spheroides* and their relation to electrical field generation across the chromatophore membrane, Eur. J. Biochem. 18 (1971) 120–130.

[74] M. Snozzi, A.R. Crofts, Electron transport in chromatophores from *Rhodopseudomonas sphaeroides* Ga fused with liposomes, Biochim. Biophys. Acta 766 (1984) 451–463.

[75] N.B. Ugulava, A.R. Crofts, CD-monitored redox titration of the Rieske Fe-S protein of *Rhodobacter sphaeroides*: pH dependence of the mid-point potential in isolated bc_1 complex and in membranes, FEBS Lett. 440 (1998) 409–413.

[76] E.J. Leggate, J. Hirst, Roles of the disulfide bond and adjacent residues in determining the reduction potentials and stabilities of respiratory-type Rieske clusters, Biochemistry 44 (2005) 7048–7058.

[77] F. Muller, A.R. Crofts, D.M. Kramer, Multiple Q-cycle bypass reactions at the Q_o-site of the cytochrome bc_1 complex, Biochemistry 41 (2002) 7866–7874.

[78] F. Muller, The nature and mechanism of superoxide production by the electron transport chain: its relevance to aging, J. Am. Aging Assoc. 23 (2000) 227–253.

[79] U. Brandt, J.G. Okun, Role of deprotonation events in ubihydroquinone: cytochrome c oxidoreductase from bovine heart and yeast mitochondria, Biochemistry 36 (1997) 11234–11240.

[80] R. Covián, R. Moreno-Sánchez, Role of protonatable groups of bovine heart bc_1 complex in ubiquinol binding and oxidation, Eur. J. Biochem. 268 (2001) 5783–5790.

[81] D.J. Kolling, J.S. Brunzelle, S. Lhee, A.R. Crofts, S.K. Nair, Atomic resolution structures of Rieske iron–sulfur protein: role of hydrogen bonds in tuning the redox potential of iron–sulfur clusters, Structure 15 (2007) 29–38.

[82] N. Seddiki, B. Meunier, D. Lemesle-Meunier, G. Brasseur, Is cytochrome *b* glutamic Acid 272 a quinol binding residue in the bc_1 complex of *Saccharomyces cerevisiae*? Biochemistry 47 (2008) 2357–2368.

[83] H. Palsdottir, C.G. Lojero, B.L. Trumpower, C. Hunte, Structure of the yeast cytochrome bc_1 complex with a hydroxyquinone anion Q_o site inhibitor bound, J. Biol. Chem. 278 (2003) 31303–31311.

[84] E.A. Berry, L.-S. Huang, D.-W. Lee, F. Daldal, K. Nagai, N. Minagawa, Ascochlorin is a novel, specific inhibitor of the mitochondrial cytochrome bc_1 complex, Biochim. Biophys. Acta. 1797 (2010) 360–370.

[85] A.R. Crofts, The mechanism of ubiquinol:cytochrome c oxidoreductases of mitochondria and of *Rhodopseudomonas sphaeroides*, in: A.N. Martonosi (Ed.), The Enzymes of Biological Membranes, Plenum Publ. Corp., New York, 1985, pp. 347–382.

[86] R. Covián, E.B. Gutierrez-Cirlos, B.L. Trumpower, Anti-cooperative oxidation of ubiquinol by the yeast cytochrome bc_1 complex, J. Biol. Chem. 279 (2004) 15040–115049.

[87] R. Covián, B.L. Trumpower, Rapid electron transfer between monomers when the cytochrome bc_1 complex dimer is reduced through center N, J. Biol. Chem. 280 (2005) 22732–22740.

[88] R. Covián, B.L. Trumpower, Regulatory interactions in the dimeric cytochrome bc_1 complex: The advantages of being a twin, Biochim. Biophys. Acta 1777 (2008) 1079–1091.

[89] P. Lanciano, D.-W. Lee, H. Yang, E. Darrouzet, F. Daldal, Intermonomer electron transfer between the low-potential *b* hemes of cytochrome bc_1, Biochemistry 50 (2011) 1651–1663.

[90] S. Hong, D. Victoria, A.R. Crofts, Inter-monomer electron transfer is too slow to compete with monomeric turnover in bc_1 complex, Biochim. Biophys. Acta 1817 (2012) 1053–1062.

[91] M. Czapla, A. Borek, M. Sarewicz, A. Osyczka, Fusing two cytochromes *b* of *Rhodobacter capsulatus* cytochrome bc_1 using various linkers defines a set of protein templates for asymmetric mutagenesis, Protein Eng. Des. Sel. 25 (2012) 15–25.

[92] B. Khalfaoui-Hassani, P. Lanciano, D.W. Lee, E. Darrouzet, F. Daldal, Recent advances in cytochrome bc_1: Inter monomer electronic communication? FEBS Lett. 586 (2012) 617–621.

[93] M. Czapla, A. Borek, M. Sarewicz, A. Osyczka, Enzymatic activities of isolated cytochrome bc_1-like complexes containing fused cytochrome *b* subunits with asymmetrically inactivated segments of electron transfer chains, Biochemistry 51 (2012) 829–835.

[94] S. Rajagukguk, S. Yang, C.A. Yu, L. Yu, B. Durham, F. Millett, Effect of mutations in the cytochrome *b* ef loop on the electron-transfer reactions of the Rieske iron–sulfur protein in the cytochrome bc_1 complex, Biochemistry 46 (2007) 1791–1798.

[95] G. Engstrom, K. Xiao, C.-A. Yu, L. Yu, B. Durham, F. Millett, Photoinduced electron transfer between the Rieske iron–sulfur protein and cytochrome c_1 in the *Rhodobacter sphaeroides* cytochrome bc_1 complex: effects of pH, temperature, and driving force, J. Biol. Chem. 277 (2002) 31072–31078.

[96] T. Wenz, R. Covian, P. Hellwig, F. MacMillan, B. Meunier, B.L. Trumpower, C. Hunte, Mutational analysis of cytochrome b at the ubiquinol oxidation site of yeast complex III, J. Biol. Chem. 282 (2006) 3977–3988.

[97] L. Zhang, Z. Li, B. Quinn, L. Yu, C.-A. Yu, Nonoxidizable ubiquinol derivatives that are suitable for the study of the ubiquinol oxidation site in the cytochrome bc_1 complex, Biochim. Biophys. Acta 1556 (2002) 226–232.

[98] K.M. Andrews, A.R. Crofts, R.B. Gennis, Large scale purification and characterization of a highly active four-subunit cytochrome bc_1 complex from *Rb. sphaeroides*, Biochemistry 29 (1990) 2645–2651.

[99] A.R. Crofts, S. Rose, Marcus treatment of endergonic reactions: a commentary, Biochim. Biophys. Acta 1767 (2007) 1228–1232.

[100] C.C. Moser, C.C. Page, R. Farid, P.L. Dutton, Biological electron transfer, J. Bioenerg. Biomembr. 27 (1995) 263–274.

[101] N. Kim, M.O. Ripple, R. Springett, Measurement of the mitochondrial membrane potential and pH gradient from the redox poise of the hemes of the bc_1 complex, Biophys. J. 102 (2012) 1194–1203.

[102] S. Ransac, N. Parisey, J.-P. Mazat, The loneliness of the electrons in the bc_1 complex, Biochim. Biophys. Acta 1777 (2008) 1053–1059.

[103] S.E. Chobot, H. Zhang, C.C. Moser, P.L. Dutton, Breaking the Q-cycle: finding new ways to study Q_o through thermodynamic manipulations, J. Bioenerg. Biomembr. 40 (2008) 501–507.

[104] A.R. Crofts, M. Guergova-Kuras, R. Kuras, N. Ugulava, J. Li, S. Hong, Proton-coupled electron transfer at the Q_o-site: what type of mechanism can account for the high activation barrier? Biochim. Biophys. Acta 1459 (2000) 456–466.

[105] I.-J. Lin, Y. Chen, J.A. Fee, J. Song, W.M. Westler, J.L. Markley, Rieske protein from *Thermus thermophilus*: ^{15}N NMR titration study demonstrates the role of iron-ligated histidines in the pH dependence of the reduction potential, J. Am. Chem. Soc. 128 (2006) 10672–10673.

[106] A. Namslauer, A.S. Pawate, R.B. Gennis, P. Brzezinski, Redox-coupled proton translocation in biological systems: Proton shuttling in cytochrome c oxidase, Proc. Natl. Acad. Sci. U. S. A. 100 (2003) 15543–15547.

[107] M. WikstrÖm, M.I. Verkhovsky, Mechanism and energetics of proton translocation by the respiratory heme-copper oxidases, Biochim. Biophys. Acta 1767 (2007) 1200–1214.

[108] P. Mitchell, Chemiosmotic Coupling and Energy Transduction, Glynn Research Ltd., Bodmin, Cornwall, 1968.

[109] P.R. Rich, The quinone chemistry of *bc* complexes, Biochim. Biophys. Acta 1658 (2004) 165–171.

[110] I. Belevich, D.A. Bloch, N. Belevich, M. Wikström, M.I. Verkhovsky, Exploring the proton pump mechanism of cytochrome c oxidase in real time, Proc. Natl. Acad. Sci. U. S. A. 104 (2007) 2685–2690.

[111] M.H.M. Olsson, P.E.M. Siegbahn, M.R.A. Blomberg, A. Warshel, Exploring pathways and barriers for coupled ET/PT in cytochrome c oxidase: A general framework for examining energetics and mechanistic alternatives, Biochim. Biophys. Acta 1767 (2007) 244–260.

[112] G. Brändén, A.S. Pawate, R.B. Gennis, P. Brzezinski, Controlled uncoupling and recoupling of proton pumping in cytochrome c oxidase, Proc. Natl. Acad. Sci. U. S. A. 103 (2006) 317–322.

[113] L. Esser, X. Gong, S. Yang, L. Yu, C.-A. Yu, D. Xia, Surface-modulated motion switch: Capture and release of iron–sulfur protein in the cytochrome bc_1 complex, Proc. Natl. Acad. Sci. U. S. A. 103 (2006) 13045–13050.

[114] D.-W. Lee, N. Selamoglu, P. Lanciano, J.W. Cooley, I. Forquer, D.M. Kramer, F. Daldal, Loss of a conserved tyrosine residue of cytochrome *b* induces reactive oxygen species production by cytochrome bc_1, J. Biol. Chem. 286 (2011) 18139–18148.

[115] E.A. Berry, L.-S. Huang, Conformationally linked interaction in the cytochrome bc_1 complex between inhibitors of the Q_o site and the Rieske iron–sulfur protein, Biochim. Biophys. Acta 1807 (2011) 1349–1363.

[116] N. Fisher, C.K. Castleden, I. Bourges, G. Brasseur, B. Meunier, Human disease-related mutations in cytochrome *b* studied in yeast, J. Biol. Chem. 279 (2004) 12951–12958.

[117] N. Fisher, B. Meunier, Re-examination of inhibitor resistance conferred by Q_o-site mutations in cytochrome *b* using yeast as a model system, Pest Manag. Sci. 61 (2005) 973–978.

[118] F. Wibrand, K. Ravn, M. Schwartz, T. Rosenberg, N. Horn, J. Vissing, Multisystem disorder associated with a missense mutation in the mitochondrial cytochrome *b* gene, Ann. Neurol. 50 (2001) 540–543.

[119] K. Rajarathnam, J. Hochman, M. Schindler, S. Ferguson-Miller, Synthesis, location, and lateral mobility of fluorescently labeled ubiquinone-10 in mitochondrial and artificial membranes, Biochemistry 28 (1989) 3168–3176.

[120] M.F. Blackwell, J. Whitmarsh, Effect of integral membrane proteins on the lateral mobility of plastoquinone in phosphatidylcholine proteoliposomes, Biophys. J. 58 (1990) 1259–1271.

[121] S. Ransac, J.-P. Mazat, How does antimycin inhibit the bc_1 complex? A part-time twin, Biochim. Biophys. Acta 1797 (2010) 1849–1857.

[122] C.C. Moser, T.A. Farid, S.E. Chobot, P.L. Dutton, Electron tunnelling chains of mitochondria, Biochim. Biophys. Acta 1757 (2006) 1096–1109.

[123] M. Eigen, Proton transfer and general acid-base catalysis, in: S. Claesson (Ed.), Fast React. Primary Processes Chem. Kinet., Proc. 5th Nobel Symp. Almqvist and Wiksell, Stockholm, Swed., 1967, pp. 245–252.

[124] R.I. Cukier, Theory and simulation of proton-coupled electron transfer, hydrogen-atom transfer, and proton translocation in proteins, Biochim. Biophys. Acta 1655 (2004) 37–44.

[125] M. Rini, B.-Z. Magnes, E. Pines, E.T.J. Nibbering, Real-time observation of bimodal proton transfer in acid-base pairs in water, Science 301 (2003) 349–352.

[126] V.P. Shinkarev, A.R. Crofts, C.A. Wraight, The electric field generated by photosynthetic reaction center induces rapid reversed electron transfer in the bc_1 complex, Biochemistry 40 (2001) 12584–12590.